Applied Mathematical Modelling 109 (2022) 651–678

Contents lists available at ScienceDirect

Applied Mathematical Modelling

journal homepage: www.elsevier.com/locate/apm

A hierarchical control scheme for multiple aerial vehicle transportation systems with uncertainties and state/input constraints

Yushu Yu[a,*], Chuanbeibei Shi[a], Dan Shan[a], Vincenzo Lippiello[b], Yi Yang[c]

[a] School of Mechatronical Engineering, Beijing Institute of Technology, Beijing 100081, China
[b] Department of Electrical Engineering and Information Technology, University of Naples Federico II, Naples 80125, Italy
[c] School of Mechatronic Engineering and Automation, Shanghai University, Shanghai 200444, China

ARTICLE INFO

Article history:
Received 27 October 2021
Revised 5 May 2022
Accepted 10 May 2022
Available online 18 May 2022

Keywords:
Multiple aerial vehicle transportation
Model predictive control
Robust invariant set
Attitude tracking error
Special Euclidean Group

ABSTRACT

Multiple aerial vehicles have the potential to transport payload in any direction and with any orientation in Special Euclidean Group. In this article, the control problem of the multiple aerial vehicle transportation system with uncertainties and state/input constraints is considered. The multiple aerial vehicles connect with the load via spherical pairs that coincide with the center of mass of the aerial vehicles. A hierarchical control scheme of such challenging complex systems is proposed. The outer loop is designed by a tube-based model predictive control in order to deal with uncertainties, state constraints and input boundedness, while the inner loop is designed by robust control technique which forces the attitude tracking error of the aircraft into robust invariant set. The attitude tracking error of the inner loop induces a difference between the commanded and the actual equivalent wrench acting on the load. Such difference is treated as the equivalent disturbance of the outer loop to guarantee the fulfillment of the state and input constraints. The hierarchical control structure simplifies the design procedure, while still preserves the convergence and feasibility of the overall controlled system under uncertainties, which are proved strictly in the paper. Numerical simulations on a six-quadrotor transportation system are conducted to demonstrate the performance of the proposed control scheme. A real-world prototype including three quadrotors is developed. The hardware-in-the-loop simulation on the prototype supports the real-time feasibility of the proposed scheme.

1. Introduction

1.1. Motivation and background

Small scale under-actuated aerial vehicles, such as quadrotors, have become ideal platforms for many applications [1]. Such vehicles are usually actuated by three torques and the total thrust. Interest in aerial manipulators based on under-actuated aerial vehicles continues to grow [2–5]. However, the payload of a single aerial vehicle for civil applications (e.g., take-off weight less than 25kg) is hard to increase also due to regulatory constraints. Moreover, the under-actuation property

* Corresponding author.
E-mail address: yushu.yu@bit.edu.cn (Y. Yu).

https://doi.org/10.1016/j.apm.2022.05.013
0307-904X/

makes the task space of the single vehicle-based aerial manipulation unable to achieve six independent Degree of Freedom (DOF). Due to the above facts, an effective manipulation capability based only on a single under-actuated aerial vehicle is limited [6]. Some researchers are trying to handle manipulation by using fully actuated vehicles [7], although such vehicles are less efficient.

Besides the fully actuated aerial vehicle, the manipulation based on multiple aerial vehicles has aroused great interests in recent years [8–10]. The multiple aerial vehicle transportation system (MAVTS), which aims at solving the 6-DOF transportation problem, is a type of multiple aerial vehicle-based manipulators. Theoretically speaking, by using the multiple aerial vehicle to provide multiple thrust, the load's attitude and position can be adjusted separately. Moreover, the load capacity can also be increased by adding additional aerial vehicles. However, as indicated by previous researchers, this is a complex system [9]. The needed controller is therefore usually endowed with a hierarchical structure, where the most inner loop is the attitude control of a single aerial vehicle. It is thus natural that the attitude tracking error of an aerial vehicle influences the stability and the performance of the entire collaborative system. An aerial vehicle suffers more uncertainties compared to a ground vehicle-based transportation system. Therefore, disturbance and uncertainty need to be explicitly considered in the control design. Moreover, the thrusts provided by aerial vehicles constitute complex combinations, which let the input force and the input torque be coupled with each other. The input constraint is therefore not easy to deal with online in the controller.

1.2. Related research

The guidance, navigation and control of autonomous vehicles is a hot topic in recent years, e.g., the autonomous vehicle collision avoidance considering multiple constraint modeling [11,12], robust control [13], the multi-objective trajectory planning [14], and the formation control of multi-UAVs [15]. Among the various methodologies, the tube-based model predictive control (MPC) has proved to be a useful technique which can deal with dynamics with uncertainties and input / state constraints [16–18]. The basic idea of the tube-based MPC can be summarized in two steps. First, the nominal state and input trajectory are generated based on the nominal dynamics. Second, a feedback control is designed. Because of the uncertainties in the system, the feedback control should be designed considering the uncertainties in such a way that the tracking error with respect to the nominal trajectory is kept in an invariant set. The MPC employed to generate the nominal trajectory should consider the previous invariant set. By using such a technique, the state and input constraints of the actual system can be incorporated. Yue et.al. adopted the tube-based MPC method to design the posture controller for tractor-trailer vehicle [19]. Gao et.al. applied tube-based MPC to the obstacle avoidance of ground vehicles [20], where the tube-based MPC has been designed based on the linearized dynamics of the bicycle model. Sun et.al. designed tube-based MPC for the simplified unicycle model, while proved the convergence and feasibility of the closed loop system [21], where the invariant set of the tracking error is proved by solving the 1st order kinematics equation of the unicycle model. Nikou et. al. proposed a control technique for the multi-agent systems by tube-based MPC [22], and designed the force control for underwater robots [23], in which the invariant set is estimated from the Lipchitz continuity of the differential equation.

The MAVTS has emerged for several years. Lee et. al. proved that a load can be transported by at least three quadrotors in SE(3) via cables [8]. Some other configurations of MAVTS have also been proposed. Via et. al. proposed a configuration composed of three aerial vehicles and three rigid links which provide connections to the load [24]. The ideas come from parallel mechanism. More specially, the attaching point between the aerial vehicle and the load is modeled as a spherical joint, and the attaching point coincides with the Center of Mass (COM) of the aerial vehicle. In this simplified configuration, the dynamics of the load is decoupled from the attitude dynamics of the aerial vehicle which provides the thrust.

The control of the multiple aerial vehicle can be divided into two categories: the centralized control and the distributed control. The former treats the entire system as an entirety, but it needs the full state information of the load and vehicles. While the latter is run in the distributed aerial vehicles, and does not reply on the information from the load and other vehicles. Cardona et. al. proposed position generation and tracking scheme for multiple quadrotor transportation system [25]. Pereira et. al. proposed a control framework for slung load transportation with two aerial vehicles [26]. Because the load is modeled as a mass point, the entire system is therefore decoupled into three subsystems, based on which the corresponding control is designed. Siegwart et.al. proposed a distributed control approach for the MAVTS [27], where the vehicles are grouped into leader and followers. The trajectory of the leader is generated offline, while the wrench acting on the aerial vehicle due to the load is provided by an estimator. From the estimated wrench information, the admittance control is used to generate the trajectory of the followers. The distributed control approach does not need communication among vehicles. However as shown in previous works, the distributed control approach is vulnerable to disturbance and its stability is difficult to be proved.

Santos et.al. proposed a controller combing tube-based MPC and nonlinear control for the load transportation with one aerial vehicle [28]. This tube-based MPC is designed based on the linearized dynamics of the load, but the feasibility analysis has not been provided.

How to estimate the robust invariant set relating to the feedback-controlled system is an important problem for the tube-based MPC. The method includes Lipchitz constant-based method [29], summers of square-based method [30–32], solutions of the differential equations [21], and reachable set-based method [20]. Fatima proposed an attractive ellipsoid control method for the aggressive motion control of quadrotor [33]. It has been noted that computation of a robust invariant set usually needs iterations and is particularly difficult for non-linear systems. However, in this paper we are inspired from

the fact that for a Lipchitz continuous system, the robust invariant set can be estimated conservatively from the Lipchitz constant.

In addition, unlike ground-based vehicles, the subspace of the configuration space of aerial vehicles includes SO(3), which is not an Euclidean space. Therefore, the configuration space of aerial vehicles is not Euclidean space. By constructing the local mapping between $SO(3)$ and the Euclidean space, the local coordinate of $SO(3)$ is obtained. Traditional methods to control the aerial vehicle are based on the equation of motion expressed by local coordinates. However, as $SO(3)$ is not global homeomorphic to Euclidean space [34], the traditional methods may suffer from various problems such as singularity and local stability. Some control schemes are investigated to avoid such problems. Mayhew and Yu et. al. proposed several hybrid control schemes for systems on non-Euclidean manifold [1,34]. Chang et. al. proposed an interesting controller for dynamics evolving on manifolds by embedding the manifold into the Euclidean space [35]. Also, Lee et. al. proposed a continuous tracking error expressed on $SO(3)$ and proposed an almost global controller for systems on $SO(3)$ based on the error function [36]. However, the design and analysis of the MPC of MAVTS considering its non-Euclidean configuration space are not well studied in the previous research.

1.3. Contributions

In this paper, we propose a control approach for MAVTS. Each aerial vehicle in the system is an under-actuated aerial vehicle. Therefore, the attitude of the vehicle is fully controllable, while the thrust of each aerial vehicle is considered as the input. We consider the control problem of transporting the load from one configuration to another one. This problem is challenging due to the following factors.

- The MAVTS is a high-order system with complex dynamics. The attitude tracking error of each aerial vehicle always exists.
- The attitude and thrust of each vehicle in the MAVTS are bounded. Besides, the unknown disturbance of the aerial vehicle is more noticeable than that of the ground vehicle. Therefore, for the MAVTS dynamics, there are state constraints and uncertainties.
- The configuration space of the MAVTS is a non-Euclidean space.

In order to solve the above challenging problems, a hierarchical control approach will be considered. The outer loop of the scheme, which controls the motion of the load, is inspired by the tube-based MPC, as it can deal with the multiple constraints. While the inner loop is a robust attitude control of the aircraft. We prove that by selecting appropriate robust control technique, the attitude tracking error of the aircraft can be bounded in a region containing origin in the presence of uncertainties. We also analyze the feasibility and convergence of the outer loop tube-based MPC taking into account the attitude tracking of the inner loop. The attitude error is expressed directly from the rotation matrix, leading to almost global stability and continuity of the attitude control. To the best knowledge of the authors, there is no similar work on the tube-based MPC for the entire MAVTS considering the input and state constraints in the presence of uncertainties.

In summary, the novelty of the proposed methodology is listed as follows.

- We propose the novel hierarchical controller structure for the entire multiple aerial vehicle transportation system considering the attitude tracking of each aerial vehicle.
- By carefully combining the tube-based MPC and the robust control, the state and the input constraints of the entire system are guaranteed in the presence of uncertainties.
- The proposed control scheme is singularity free and globally effective because the attitude is not represented by any local coordinates.
- The convergence and feasibility of the entire complex system are analyzed mathematically.

This paper is organized as follows. The modeling of the MAVTS and the problem formulation is presented in Section 2. The overall control structure is designed in Section 3, where the robust inner-loop control and the feedback outer-loop control are designed and analyzed. In Section 4, both the convergence and feasibility of the entire controlled system are demonstrated. Finally, numerical simulation results and discussion on the real-world implementation are presented in Section 5.

2. Modeling and problem formulation

2.1. Configuration of multiple aerial vehicle transportation system

The MAVTS in this paper is composed of a load and multiple aerial vehicles, where the aerial vehicles provide the thrust for lifting the load. The configuration of the entire system is shown in Fig. 1. The multiple aerial vehicle is connected with the load via spherical joints. In this paper, we assume that the COM of the aerial vehicle is in the center of the spherical joints.

Under such a configuration, each aerial vehicle can rotate about the passive spherical joint with its rotation dynamics. Therefore, the aerial vehicle can adjust its attitude and the thrust magnitude, i.e., the thrust vector. By adjusting the thrust vector coordinately, the attitude and position of the load can be adjusted simultaneously. For a system with n aerial vehicles, it is seen that the DOF of the entire system is $6+n$, as the translational motion of each vehicle is dependent on the

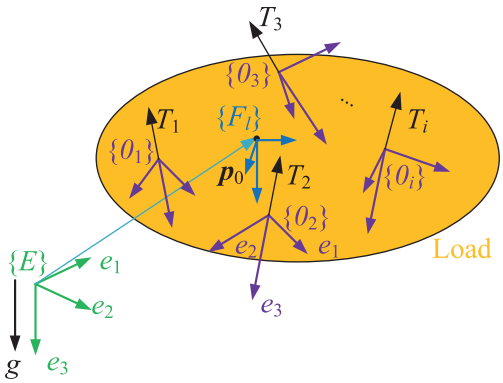

Fig. 1. The configuration of the multiple aerial vehicle transportation system. The COM of each aerial vehicle coincides with the center of the spherical joint. The thrust of each aerial vehicle points along the negative direction of $R_i e_3$.

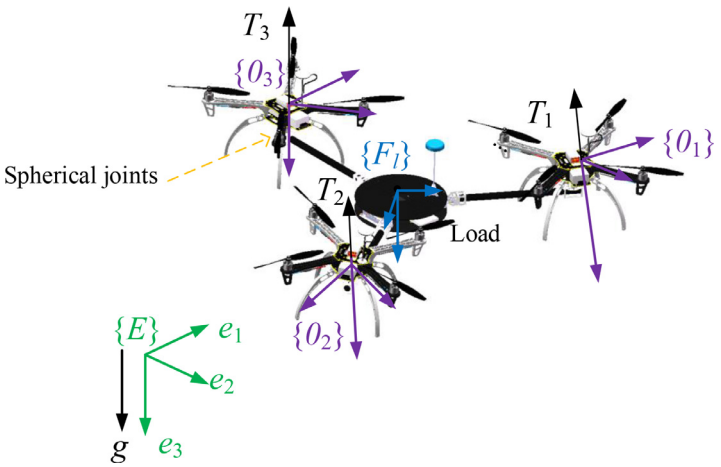

Fig. 2. An example structure of a multiple aerial vehicle transportation system prototype containing three aerial vehicles. There is no cable to connect the payload and spherical hinge in the system. Each vehicle connects with the payload with a spherical joint. Each vehicle can provide a thrust vector.

Fig. 3. The rotational range of a spherical joint.

translational motion of the load, while the rotational motion of each vehicle is independent from the load. Also, it has been proved in the previous paper that if $n \geq 3$ and the vehicles are not in a line, then the load is six-DOF fully actuated [8,9].

It is noted that the attitude and the thrust magnitude of all the aerial vehicles are all bounded, because the range of the spherical joint is bounded as seen in Fig. 3. Besides, for the real vehicle there is inevitably offset between the COM of the aerial vehicle and the center of the spherical joint. And for the aerial vehicle, the external disturbance always exists. As seen later in this section, such factors will be regarded as disturbances in the modeling.

Table 1
Notations in the system modeling.

Notations	Definition
$V_0 \in \mathbb{R}^6$	velocity of COM of the entire system
$v_0 \in \mathbb{R}^3$	linear velocity of COM of the entire system
$\omega_0 \in \mathbb{R}^3$	angular velocity of COM of the entire system
$\mathcal{M} \in \mathbb{R}^{6\times6}$, $\mathcal{C} \in \mathbb{R}^{6\times6}$, $\mathcal{G} \in \mathbb{R}^6$	the mass matrix, Coriolis matrix and the gravity matrix
$a \in \mathbb{R}^3$	vector
$R_0 \in SO(3)$	the rotation matrix representing the attitude of the load
$d_0 \in \mathbb{R}^6$	the uncertainties in the load dynamics
$m_i \in \mathbb{R}$	the mass of ith vehicle
$m_0 \in \mathbb{R}$	the mass of the load
$M_0 \in \mathbb{R}^{3\times3}$	the inertia tensor of the load
$g \in \mathbb{R}$	the acceleration due to gravity
$w_i \in \mathbb{R}^3$	the position of ith vehicle in $\{F_l\}$
$w_c \in \mathbb{R}^3$	the position of COM of the complete system in $\{F_l\}$
$b_{0,r} \in \mathbb{R}$, $b_{0,t} \in \mathbb{R}$	the upper bound of disturbance on load
$p_0 \in \mathbb{R}^3$	the position of the COM of the entire system
$R_i \in SO(3)$, $\omega_i \in \mathbb{R}^3$	the attitude and the angular velocity of ith vehicle
$\tau_i \in \mathbb{R}^3$	the input torque for ith vehicle
$d_{i,t} \in \mathbb{R}^3$	the translational uncertainties for ith vehicle
$d_{i,r} \in \mathbb{R}^3$	the rotational uncertainties for ith vehicle
$b_a \in \mathbb{R}$	the upper bound of each vehicle
$\Upsilon_i \in \mathbb{R}^3$	the thrust vector provided by ith vehicle
B	the allocation matrix
x	the state vector of the entire system
$T_i \in \mathbb{R}$	the thrust magnitude of vehicle-i
$M_i \in \mathbb{R}^{3\times3}$	the inertia tensor of vehicle-i
$\omega_i \in \mathbb{R}^3$	the angular velocity of vehicle-i
$v_i \in \mathbb{R}^3$	the linear velocity of vehicle-i
$N_i \in \mathbb{R}^3$	the constraint force in joint-i
$\zeta = (p_{0,e}, R_{0,e}, V_0)$	the state relating to error of load
$y = (p_0, R_0, V_0)$	the state relating to load

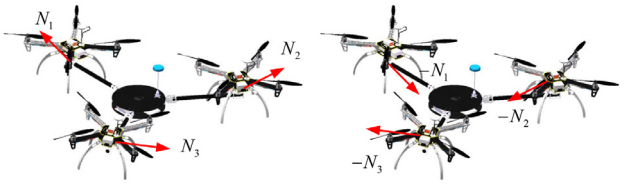

Fig. 4. The constraint force exerted on each aerial vehicle (left) and the load (right). N_i is expressed in world frame $\{E\}$.

2.2. Modeling of multiple aerial vehicle transportation system

For a system containing n aerial vehicles, we can define a world frame $\{E\}$, the load body-fixed frame $\{F_c\}$ whose origin locates at the COM of the entire system, and the load's body-fixed frame $\{F_l\}$ whose origin locates at the COM of the load. We also consider body-fixed frames $\{O_i\}, i = 1, 2, \cdots, n$ to each aerial vehicle. It is seen that the two frames $\{F_l\}$ and $\{F_c\}$ are parallel. And as the COM of each aerial vehicle coincides with the spherical joint center, the distance between the two frames $\{F_l\}$ and $\{F_c\}$ keeps constant. The offset between the COM of each aerial vehicle and the spherical joint center is treated as modeling uncertainties. The notations in the modeling are listed in Table 1.

Each aerial vehicle is an under-actuated aerial vehicle, which means each vehicle is actuated by the 3-D torque $\tau_i \in \mathbb{R}^3$ and 1-D thrust $T_i \in \mathbb{R}$. The direction of T_i is fixed in the body frame of the aerial vehicle, and points to the negative direction of $R_i e_3$, where $R_i \in SO(3)$ expresses the attitude of vehicle-i, and $e_3 = (0, 0, 1)^T$. Therefore, the thrust vector provided by ith vehicle expressed in the load frame is written by,

$$\Upsilon_i = R_0^T R_i e_3 T_i, \tag{1}$$

where $R_0 \in SO(3)$ expresses the attitude of load.

The spherical joint connecting the aerial vehicle and the load induces the constraint force. As the vehicle can rotate freely around the spherical joint, it is assumed that only the constraint force exists and there is no constraint torque. The constraint force is denoted by $N_i \in \mathbb{R}^3$ expressed in $\{E\}$. As seen in Fig. 4, the constraint forces exerted on the load and that exerted on the aerial vehicle are reacting forces.

Besides, in modeling the system, there is disturbance acting on each aerial vehicle and the load. The disturbance is induced by the offset between the center of the spherical joint and the COM of each vehicle, the friction force of the

spherical joints, the parameter errors, the wind disturbance, etc. It is reasonable to assume that the disturbance d_i for vehicle-i is bounded.

For vehicle-i, with $i = 1, 2, \cdots, n$, it suffers from the gravity force, the constraint force, the input thrust and torque, and the disturbances. By applying Newton-Euler's law, the dynamics of each vehicle can be written as,

$$\dot{v}_i = -\frac{1}{m_i}\hat{\omega}_i v_i + g R_i^T e_3 + \frac{1}{m_i} R_i^T N_i - \frac{1}{m_i} R_i^T R_0 \Upsilon_i + d_{i,t} \tag{2a}$$

$$\dot{\omega}_i = M_i^{-1}(-\hat{\omega}_i M_i \omega_i + \tau_i) + d_{i,r} \tag{2b}$$

where m_i represents the mass of ith vehicle, $M_i \in \mathbb{R}^{3\times3}$ is the inertia tensor of ith vehicle, $v_i \in \mathbb{R}^3$ is the linear velocity of ith vehicle expressed in frame $\{O_i\}$, $\omega_i \in \mathbb{R}^3$ is the angular velocity of ith vehicle expressed in frame $\{O_i\}$, $\tau_i \in \mathbb{R}^3$ represents the bounded input toque for ith vehicle, $d_{i,t} \in \mathbb{R}^3$ and $d_{i,r} \in \mathbb{R}^3$ represent the bounded disturbance for ith vehicle induced by the uncertainties and external disturbances, g is the acceleration due to gravity, and the hat map $\hat{a}$ for a vector $a = (a_1, a_2, a_3)^T \in \mathbb{R}^3$ is defined by

$$\hat{a} = \begin{bmatrix} 0 & -a_3 & a_2 \\ a_3 & 0 & -a_1 \\ -a_2 & a_1 & 0 \end{bmatrix} \tag{3}$$

Similarly, the dynamics of the load can be expressed as,

$$\dot{v}_0 = g e_3 - \frac{1}{m_0}\Sigma_{i-1}^n N_i + d_{0,t} \tag{4a}$$

$$\dot{\omega}_0 = -M_0^{-1}\hat{\omega}_0 M_0 \omega_0 - M_0^{-1}\Sigma_{i=1}^n \hat{w}_i R_0^T N_i + d_{0,r} \tag{4b}$$

where $v_0 \in \mathbb{R}^3$ is the linear velocity expressed in frame $\{E\}$, $\omega_0 \in \mathbb{R}^3$ is the angular velocity expressed in frame $\{F_l\}$, m_0 represents the mass of the load, M_0 represents the inertia tensor of the load, expressed in $\{F_l\}$, $w_i \in \mathbb{R}^3$ is the position of ith vehicle in $\{F_l\}$, $d_{0,t} \in \mathbb{R}^3$ and $d_{0,r} \in \mathbb{R}^3$ represent the bounded disturbance.

Because of the connection of the spherical joints, the position of the vehicles and load at the connecting point should be the same, which can be written as the following equation,

$$p_i = p_l + R_0 w_i, i = 1, 2, \cdots, n \tag{5}$$

where $p_i \in \mathbb{R}^3$ is the origin of frame $\{O_i\}$ expressed in the world frame $\{E\}$, $p_l \in \mathbb{R}^3$ is the origin of frame $\{F_l\}$ expressed in the world frame $\{E\}$.

Inserting (2a) into (4a) and (4b), then applying (5) and the time derivative of (5), the constraint force N_i can be eliminated in (4a) and (4b). Equation (4a) and (4b) can thus be simplified into the following format [9],

$$\mathcal{M}\dot{V}_0 + \mathcal{C}V_0 + \mathcal{G} = \begin{bmatrix} R_0 & 0 \\ 0 & I \end{bmatrix} u_0 + d_0 \tag{6}$$

where $V_0 := (v_0, \omega_0) \in \mathbb{R}^6$ represents the velocity of the COM of the entire system, $\mathcal{M} \in \mathbb{R}^{6\times6}$, $\mathcal{C} \in \mathbb{R}^{6\times6}$, $\mathcal{G} \in \mathbb{R}^6$ are the mass matrix, Coriolis matrix, and the gravity matrix respectively, $u_0 \in \mathbb{R}^6$ is the equivalent wrench acting on the load expressed in $\{F_c\}$, I is the identity matrix, and $d_0 \in \mathbb{R}^6$ represents the bounded uncertainties.

The expression of the mass matrix, Coriolis matrix, and the gravity matrix is written as follows:

$$\begin{aligned} &\mathcal{M} = \begin{bmatrix} m_t & 0 \\ 0 & M_t \end{bmatrix}, \quad \mathcal{C} = \begin{bmatrix} 0 & 0 \\ 0 & -(M_t\omega_0)\hat{} \end{bmatrix}, \\ &\mathcal{G} = \begin{bmatrix} m_t g e_3 \\ 0 \end{bmatrix} \end{aligned} \tag{7}$$

with

$$m_t = \sum_{i=0}^{n} m_i, M_t = M_0 - \sum_{i=1}^{n} m_i \hat{w}_i(\hat{w}_i - \hat{w}_c) \tag{8}$$

where $w_c \in \mathbb{R}^3$ is the position of COM of the complete system in $\{F_l\}$.

We express the boundedness of $d_0 = (d_{0,t}^T, d_{0,r}^T)^T$ by

$$\|d_{0,t}\| \le b_{0,t}, \|d_{0,r}\| \le b_{0,r} \tag{9}$$

where $b_{0,t}$ and $b_{0,r}$ are positive constants.

It is seen that EOM (6) is the dynamics expressed by the COM of the entire system. As we assume the center of each aerial vehicle coincides with the joint center, the inertia matrix in (6) is constant, such EOM is actually similar to that of a rigid body with disturbances. As seen later in the controller design, this property will simplify the design procedure.

The kinematics of the load is governed by the following equation

$$\dot{p}_0 = v_0, \quad \dot{R}_0 = R_0\hat{\omega}_0 \tag{10}$$

where $p_0 \in \mathbb{R}^3$ represents the position of the COM of the entire system.

As introduced earlier, the rotational motion of each aerial vehicle is independent from the motion of the load. To fully describe the motion of the entire system, the equation of the rotational motion of each aerial vehicle is needed. For ith vehicle, the rotational motion is governed by the following equation,

$$\dot{R}_i = R_i\hat{\omega}_i, \dot{\omega}_i = M_i^{-1}(\tau_i - \hat{\omega}_i M_i\omega_i) + d_{i,r} \tag{11}$$

And the boundedness of $d_{i,r}$ is expressed by

$$\|d_{i,r}\| \le b_a \tag{12}$$

where b_a is a positive constant.

The equivalent input wrench in (6) is expressed as,

$$u_0 = \begin{bmatrix} I & I & \cdots & I \\ \hat{l}_1 & \hat{l}_2 & \cdots & \hat{l}_n \end{bmatrix} \begin{bmatrix} \Upsilon_1 \\ \Upsilon_2 \\ \cdots \\ \Upsilon_n \end{bmatrix} := B\Upsilon \tag{13}$$

where $l_i = w_i - w_c$ with $i = 1, 2, \cdots, n$.

Equations (6), (10) and (11) constitute the equation of motion (EOM) of the entire system of the MAVTS. The state of such a system can be defined as $x := (p_0, R_0, V_0, R_i, \omega_i) \in SE(3) \times \mathbb{R}^6 \times SO(3) \times \mathbb{R}^3 \cdots \times SO(3) \times \mathbb{R}^3$. The state relating to the load is defined as $y = (p_0, R_0, V_0) \in SE(3) \times \mathbb{R}^6$.

Assumption 1. The aircraft can rotate around the spherical joint. The home attitude of the aircraft is $R_0^T R_i = I$, and the feasible relative attitude of the aircraft is expressed as

$$U_j = \{R_i : e_3^T R_0^T R_i e_3 \ge L_c\} \tag{14}$$

where $L_c < 1$ is a positive constant which defines the range of the spherical joint. The thrust magnitude of each aircraft satisfies $T_i < T_m$, where $T_m > 0$ is a positive constant.

2.3. Problem formulation

In this paper we will consider the control problem of the MAVTS subjecting to state constraints and input boundedness. While for this system, we are more concerned with how the load can be transported to the desired configuration. The control problem can therefore be expressed as follows.

Problem 1. Consider the MAVTS governed by the EOM (6), (10) and (11). Suppose the state and input of the system are subject to Assumption 1, specific configuration constraints $(p_0, R_0) \in \mathcal{X}$, and specific velocity constraints $V_0 \in \mathcal{V}$. Given desired load configuration $p_{0,d}$ and $R_{0,d}$, deign control input $(\tau_i, T_i) : t \mapsto (\tau_i, T_i)$ which forces $\|p_0 - p_{0,d}\| \le c_1$ and $\|\exp^{-1}(R_{0,d}^T R_0)\| \le c_2$ as $t \to \infty$ with small positive constant c_1 and c_2, while fulfilling all the above constraints for all disturbance satisfying (9) and (12).

Remark 1. The desired position and velocity in Problem 1 is the position and velocity of the COM of the entire system. During transportation, usually we are more concerned with the position and velocity of the load's COM. However, as the center of the spherical joint coincides with the COM of the aerial vehicles, the COM of the entire system keeps constant in $\{F_l\}$. Hence the desired position / velocity of the load's COM can be easily transformed into the desired state y_d.

From Assumption 1, the admissible thrust set provided by each aerial vehicle expressed in $\{F_c\}$ can be written as $U_T = \{\Upsilon_i \in \mathbb{R}^3 : \|\Upsilon_i\| \le T_m, \frac{\Upsilon_i^T}{\|\Upsilon\|} e_3 \le -L_c\}$. And one can define the feasible set of the equivalent wrench u_0 as,

$$\begin{aligned} S_\tau &= \{\tau \in \mathbb{R}^3 : \tau = \textstyle\sum \hat{l}_i R_0^T R_i T_i e_3, R_i \in U_j, 0 < T_i < T_m\} \\ S_F &= \{F \in \mathbb{R}^3 : F = \textstyle\sum R_0^T R_i T_i e_3, R_i \in U_j, 0 < T_i < T_m\} \end{aligned} \tag{15}$$

However, it is seen that S_τ and S_F are dependent from each other. In order to explore the feasibility of the system, it is therefore necessary to construct an admissible set U_w. It is defined that for all $u_0 \in U_w$, the solution thrust Υ always exists. We have the following lemma.

Lemma 1. *Consider the MAVTS, the wrench acting on the load generated by the multiple thrust is expressed by (13). There exist positive constants τ_m, $F_{m,h}$ and $F_{m,z}$, such that for all $u_0 = (F_0, \tau_0) \in \{\tau_0 = (\tau_{0,x}, \tau_{0,y}, \tau_{0,z})^T \in \mathbb{R}^3 : \|\tau_0\| \le \tau_m\} \times \{F_0 = (F_{0,x}, F_{0,y}, F_{0,z})^T \in \mathbb{R}^3 : F_{0,x}^2 + F_{0,y}^2 \le F_{m,h}^2, |F_{0,z} + m_t g| \le F_{m,z}\}$, the solution $\Upsilon_i \in U_T$ of the equation $B\Upsilon = u_0$ exists.*

Proof. From the configuration of the system, it is seen that $\tau_{0,z}$ is only affected by $\Upsilon_i^T e_1$ and $\Upsilon_i^T e_2$, where $e_1 = (1, 0, 0)^T$ and $e_2 = (0, 1, 0)^T$. Similarly, it is seen that $\tau_{0,x}$ and $\tau_{0,y}$ are only decided by $\Upsilon_i^T e_3$. This means that the feasible set of

$(F_{0,x}, F_{0,y}, \tau_{0,z})^T$ is independent from the feasible set of $(\tau_{0,x}, \tau_{0,y}, F_{0,z})^T$. Therefore, from U_j the independent admissible set of $(F_{0,x}, F_{0,y}, \tau_{0,z})$ and $(\tau_{0,x}, \tau_{0,y}, F_{0,z})$ can be obtained. Let S_1 and S_2 denote the feasible set of $(F_{0,x}, F_{0,y}, \tau_{0,z})$ and $(\tau_{0,x}, \tau_{0,y}, F_{0,z})$ respectively. In this context, we can construct two maximum cylinders inside S_1 and S_2 respectively, $S_3 = \{(F_{0,x}, F_{0,y}, \tau_{0,z}) \in S_1 : F_{0,x}^2 + F_{0,y}^2 \le r_1, \|\tau_{0,z}\| \le r_2\}, S_4 = \{(\tau_{0,x}, \tau_{0,y}, F_{0,z}) \in S_2 : \tau_{0,x}^2 + \tau_{0,y}^2 \le r_3, |F_{0,z} + m_t g| \le r_4\}$ where r_1, r_2, r_3, and r_4 are positive constants. It is seen that S_3 and S_4 are also independent and feasible. Then the following independent feasible force and torque set can be constructed,

$$\begin{aligned} S_5 = &\quad \{F_0 : F_{0,x}^2 + F_{0,y}^2 \le r_1, |F_{0,z} + m_t g| \le r_4\}, \\ S_6 = &\quad \{\tau_0 : \tau_{0,x}^2 + \tau_{0,y}^2 \le r_3, |\tau_{0,z}| \le r_2\}, \end{aligned} \tag{16}$$

We define $F_{m,h} = \sqrt{r_1}$, $F_{m,z} = r_4$, $\tau_m = \min(r_2, \sqrt{r_3})$, and define $S_7 = \{\tau_0 : \|\tau_0\| \le \tau_m\}$, which is the maximum sphere inside S_6. Finally, the feasible wrench set can be expressed as,

$$U_w = S_5 \times S_7 \tag{17}$$

As S_5 and S_7 are independent from each other, for all $u_0 \in U_w$, the solution Υ to the equation $B\Upsilon = u_0$ exists. This completes the proof. □

Lemma 2. *[37] The following inequality holds for any $\epsilon > 0$ and for any $\eta \in \mathbb{R}$,*

$$0 \le |\eta| - \eta \tanh\left(\frac{\eta}{\epsilon}\right) \le k_t \epsilon \tag{18}$$

where k_t is a constant satisfying $k_t = e^{-(k_t+1)}$, i.e., $k_t = 0.2785$.

3. Overall controller structure

3.1. Nominal tracking error dynamics

Given the desired configuration of the load, we can define the tracking error dynamics of the system. Letting $p_{0,d}$ and $R_{0,d}$ represent the desired constant position and rotation matrix of the load, respectively, and letting the desired velocity be zeros, we can express the configuration error of the system as,

$$p_{0,e} = p_0 - p_{0,d}, R_{0,e} = R_0^T R_{0,d} \tag{19}$$

The dynamics of the multiple thrust vector load system can thus be rewritten with the above variables as,

$$\begin{aligned} \dot{p}_{0,e} &= v_0 \\ \dot{R}_{0,e} &= R_{0,e}^T \hat{\omega}_0 \\ \dot{v}_0 &= g e_3 + \tfrac{1}{m_t} R_0 F_0 + d_{0,t} \\ \dot{\omega}_0 &= M_t^{-1}(\tau_0 - \omega_0 \times M_t \omega_0) + d_{0,r} \end{aligned} \tag{20}$$

In this paper, the tube-based MPC for the MAVTS will be designed. The nominal dynamics is the basis of the tube-based MPC design. In order to finish the design procedure, first we write the nominal dynamics of the system by eliminating the disturbance from (20),

$$\begin{aligned} \dot{\bar{p}}_{0,e} &= \bar{v}_0 \\ \dot{\bar{R}}_{0,e} &= \bar{R}_{0,e}^T \hat{\bar{\omega}}_0 \\ \dot{\bar{v}}_0 &= g e_3 + \tfrac{1}{m_t} \bar{R}_0 \bar{F}_0 \\ \dot{\bar{\omega}}_0 &= M_t^{-1}(\bar{\tau}_0 - \bar{\omega}_0 \times M_t \bar{\omega}_0) \end{aligned} \tag{21}$$

The computational complexity of MPC makes it not suitable to run in high frequency, which is needed for the attitude control of aerial vehicles. In order to reduce the computation burden, the control of the aerial vehicle is designed using adaptive control technique. As the dynamics of each aerial vehicle is decoupled from the dynamics of the load, the attitude control of the aerial vehicle is the inner loop in the entire controller. It is natural that the outer loop tube-based MPC is possible to guarantee the state constraints and input boundedness under the uncertainties, if the attitude tracking error of the aerial vehicle is bounded. The entire control system is shown in Fig. 5.

3.2. Robust attitude control of aerial vehicles

In order to solve the formulated problem, each aerial vehicle should be able to track the attitude commands in the presence of input boundedness and external disturbances. It is noted that the input boundedness can also be treated as disturbance if it is appropriately modeled. In this paper, we divide the attitude control of each aerial vehicle into two loops, the outer loop is designed for the attitude kinematics, while the inner loop is designed for the attitude dynamics.

Let the desired closed outer loop of the attitude controller be

$$\dot{e}_{R,i} = -k_{i,1} e_{R,i} \tag{22}$$

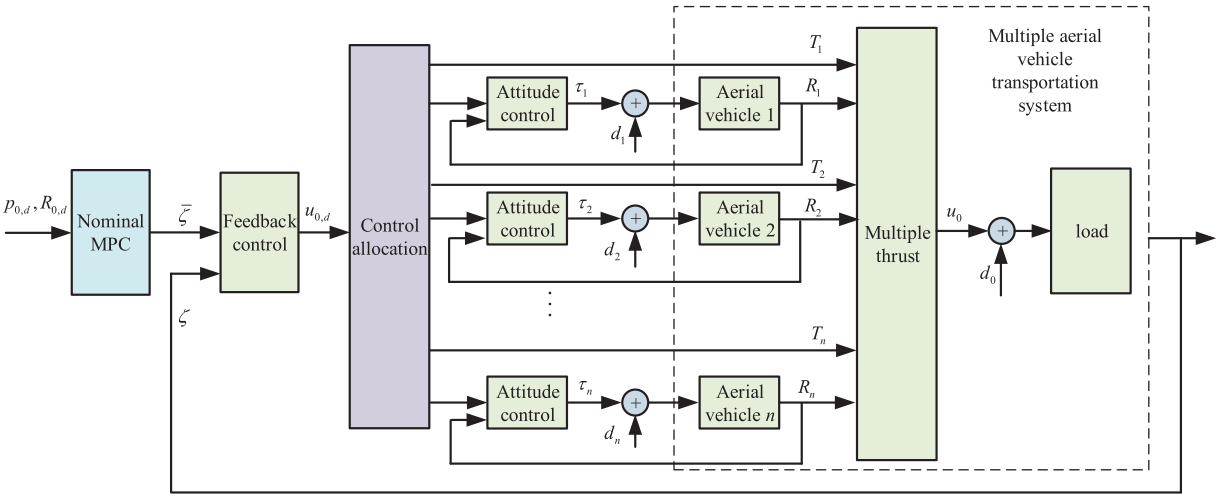

Fig. 5. The overall control block.

where $k_{i,1}$ is a positive constant, and $e_{R,i} = \frac{1}{2}(R_i^T R_{i,d} - R_{i,d}^T R_i)^\vee$ is the attitude error between the commanded attitude and actual attitude of ith vehicle, $so(3) \ni a \mapsto a^\vee \in \mathbb{R}^3$ is the vee map which is the inverse of the hat map.

Therefore, the outer loop of the attitude control is designed as,

$$\bar{\omega}_i = (\bar{R}_i^T \dot{\bar{R}}_i)^\vee - k_{i,1} e_{R,i} \tag{23}$$

The desired closed inner loop of the attitude controller is

$$\dot{\tilde{\omega}}_i = -k_{i,2} \tilde{\omega}_i \tag{24}$$

where $k_{i,2}$ is a positive gain, and $\tilde{\omega}_i = \omega_i - \bar{\omega}_i$.

Considering the external disturbances, the controller for the inner loop of the attitude controller is thus designed as,

$$\tau_i = M_i \left(\dot{\bar{\omega}}_i - k_{i,2} \tilde{\omega}_i - b_a^* \tanh\left(\frac{\tilde{\omega}_i}{\epsilon} \right) \right) + \hat{\omega}_i M_i \omega_i \tag{25}$$

where the adaptive term b_a^* is estimated by the following adaptive law,

$$\dot{b}_a^* = \frac{1}{\kappa_1} \tilde{\omega}_i \tanh\left(\frac{\tilde{\omega}_i}{\epsilon_1} \right) - \gamma_1 b_a^* \tag{26}$$

where κ_1 and γ_1 are positive gains, and ϵ_1 is a small constant.

Proposition 1. *Consider the aerial vehicle system whose rotational motion is governed by (11), and the control law is given by (25). Suppose the attitude error of the aircraft satisfies* $\frac{1}{2}\mathrm{tr}(I - R_d^T R) < 2$. *If the control gains in the controller are appropriately selected, then the closed loop tracking error* $(e_{R,i}, \tilde{\omega}_i)$, *and the disturbance estimation error* $\tilde{b}_a = b_a - b_a^*$ *converge to a small region containing origin in finite time.*

Proof. See Appendix A in supplementary document. □

3.3. Equivalent disturbance induced by the attitude tracking error of aircraft

Lemma 3. *Consider the MAVTS (6), (10) and (11). The equivalent wrench to the load is given by (13). The attitude control of the under-actuated vehicle is given by (25). Then the difference between the actual equivalent input* $u_0 = (F_0, \tau_0)$ *and the desired equivalent input* $u_{0,d} = (F_{0,d}, \tau_{0,d})$ *is bounded.*

Proof. From Proposition 1, it has been shown that the attitude tracking error of the aerial vehicles is bounded in a region containing origin. We can express the boundedness as $\|R_i - \bar{R}_i\| \le \Delta_R$, where Δ_R is a positive constant. Then it can be concluded that the difference between the commanded thrust vector and actual thrust vector provided by each aerial vehicle satisfies,

$$\|\Upsilon_i - \bar{\Upsilon}_i\| = \|R_0^T R_i T_i e_3 - R_0^T \bar{R}_i T_i e_3\| \le T_i \|R_i - \bar{R}_i\| \le T_m \Delta_R \tag{27}$$

From (13), it is seen that the difference between the desired force and actual force acting on the load satisfies,

$$\begin{array}{ll} \|F_0 - F_{0,d}\| = & \left\|\sum_i (\Upsilon_i - \bar{\Upsilon}_i)\right\| \le \sum \|\Upsilon_i - \bar{\Upsilon}_i\| \\ \le & \sum T_m \Delta_R := L_F \end{array} \tag{28}$$

Similarly, the difference between the actual and the desired equivalent moment acting on the load is bounded as,

$$\begin{array}{l} \|\tau_0 - \tau_{0,d}\| = \left\|\sum \hat{l}_i(\Upsilon_i - \bar{\Upsilon}_i)\right\| \le \sum \|\hat{l}_i(\Upsilon_i - \bar{\Upsilon}_i)\| \le \\ \sum \|l_i\| \|\Upsilon_i - \bar{\Upsilon}_i\| := L_\tau \end{array} \tag{29}$$

□

From Lemma 3, we can actually treat the difference between the desired thrust and the actual thrust induced by the attitude tracking error as disturbance. The EOM of the entire system expressed in error can thus be written as,

$$\begin{array}{ll} \dot{p}_{0,e} & = v_0 \\ \dot{R}_{0,e} & = R_{0,e}^T \hat{\omega}_0 \\ \dot{v}_0 & = g e_3 + \frac{1}{m_t} R_0 F_{0,d} + d_t \\ \dot{\omega}_0 & = M_t^{-1}(\tau_{0,d} - \omega_0 \times M_t \omega_0) + d_r \end{array} \tag{30}$$

where $d_t = d_{0,t} + d_{a,t}$, $d_r = d_{0,r} + d_{a,r}$, $d_{a,t}$ and $d_{a,r}$ are the disturbance induced by the attitude tracking error of the aircrafts. The disturbance d_t and d_r can thus be bounded as,

$$\|d_r\| \le b_{0,r} + L_\tau := b_r, \quad \|d_t\| \le b_{0,t} + L_F := b_t \tag{31}$$

3.4. Feedback control of the load dynamics

For the nominal load dynamics, suppose there exists a nominal state trajectory $\bar{\zeta}(t) = (\bar{p}_{0,e}, \bar{R}_{0,e}, \bar{v}_0, \bar{\omega}_0)$ and corresponding nominal input trajectory $\bar{u}_0(t)$, one step for the tube-based MPC is to design a feedback control law to force the trajectory of the load track the nominal trajectory, and the tracking error should be kept in a robust invariant set, which is defined as the tube of the tracking error. For this purpose, we will design the feedback control law for the load attitude and position tracking, respectively.

A cascaded structure controller will be considered for the load attitude control purpose. First, we design the following reference angular velocity for the feedback attitude control,

$$\omega_{0,r} = \bar{\omega}_0 - k_1 e_{\tilde{R},0} \tag{32}$$

where $e_{\tilde{R},0} = \frac{1}{2}(\bar{R}_{e,0}^T R_{e,0} - R_{e,0}^T \bar{R}_{e,0})^\vee$ is the attitude error between $\bar{R}_{e,0}$ and $R_{e,0}$, and k_1 is a positive constant.

Then design the body torque as,

$$\tau_{0,d} = \tau_{0,r} - k_2 e_{\omega,0} \tag{33}$$

where $e_{\omega,0} = \omega_0 - \omega_{0,r}$, $\tau_{0,r} = M_t \dot{\omega}_{0,r} + \hat{\omega}_{0,r} M_t \omega_{0,r}$, and k_2 is a positive constant.

From the load translational EOM, the feedback position control law for the load is designed as,

$$F_{0,d} = \bar{F}_0 - k_3 \tilde{p}_{0,e} - k_4 \tilde{v}_0 \tag{34}$$

where k_3 and k_4 are positive constants, $\tilde{p}_{0,e} = p_{0,e} - \bar{p}_{0,e}$ and $\tilde{v}_0 = v_0 - \bar{v}_0$ are the corresponding position and velocity tracking error of the load.

Let us consider the tracking error of the angular velocity of the load, substituting (32) into (30) we have,

$$\begin{array}{ll} \dot{e}_{\omega,0} = & M_t^{-1}\tau_0 - M_t^{-1}\hat{\omega}_0 M_t \omega_0 - M_t^{-1}\tau_{0,r} + M_t^{-1}\hat{\omega}_{0,r} M_t \omega_{0,r} \\ = & M_t^{-1}(\tau_0 - \tau_{0,r}) + M_t^{-1}\hat{\omega}_{0,r} M_t \omega_{0,r} - M_t^{-1}\hat{\omega}_0 M_t \omega_0 \end{array} \tag{35}$$

Define a function $\eta_1(\omega) : \{\omega \in \mathbb{R}^3 : \|\omega\| \le \omega_m\} \ni \omega \mapsto M_t^{-1}\hat{\omega} M_t \omega \in \mathbb{R}^3$ with positive constant ω_m, then we have,

$$\|\eta_1(\omega_0) - \eta_1(\omega_{0,r})\| \le L_1 \|e_{\omega,0}\| \tag{36}$$

where L_1 is the Lipchitz constant of the function $\eta_1(\omega)$.

Similarly, substituting the control law (34) into the EOM of load (30) yields,

$$\begin{array}{ll} \dot{\tilde{v}}_0 = & \dot{v}_0 - \dot{\bar{v}}_0 = \frac{1}{m_t} R_0 F_{0,d} - \frac{1}{m_t} \bar{R}_0 \bar{F}_{0,d} + d_t \\ = & \frac{1}{m_t} R_0 F_{0,d} - \frac{1}{m_t} \bar{R}_0 F_{0,d} + \frac{1}{m_t} \bar{R}_0 F_{0,d} - \frac{1}{m_t} \bar{R}_0 \bar{F}_0 + d_t \\ = & \frac{1}{m_t} R_0 F_{0,d} - \frac{1}{m_t} \bar{R}_0 F_{0,d} + \frac{1}{m_t} \bar{R}_0 (-k_3 \tilde{p}_{e,0} - k_4 \tilde{v}_0) + d_t \end{array} \tag{37}$$

Moreover, we have

$$\left\| \frac{1}{m_t} R_0 F_{0,d} - \frac{1}{m_t} \bar{R}_0 F_{0,d} \right\| \le \frac{1}{m_t} \|F_{0,d}\| \|R_0 - \bar{R}_0\| \le L_2 \|e_{\tilde{R},0}\| \tag{38}$$

where L_2 is a positive constant because of the boundedness of $F_{0,d}$.

In order to derive the results, we further define $\eta_2(\omega) : \{\omega \in \mathbb{R}^3 : \|\omega\| \leq \omega_m\} \ni \omega \mapsto \hat{\omega} M_t \omega \in \mathbb{R}^3$, hence we have

$$\|\eta_2(\omega_{0,r}) - \eta_2(\bar{\omega}_0)\| \leq L_3 \|\omega_{0,r} - \bar{\omega}_0\| \leq L_3 k_1 \|e_{\tilde{R},0}\| \tag{39}$$

where L_3 is the Lipchitz constant of $\eta_2(\cdot)$.

Besides $e_{\tilde{R}_0}$, $\tilde{p}_{0,e}$ and $\tilde{v}_0$, we define the angular velocity tracking error, and the error between the nominal input and actual input as,

$$\tilde{\omega}_0 = \omega_0 - \bar{\omega}_0, \tilde{\tau}_0 = \tau_{0,d} - \bar{\tau}_0, \tilde{F}_0 = F_{0,d} - \bar{F}_0 \tag{40}$$

Then we have the following proposition.

Proposition 2. *Consider the load dynamics (30). The nominal state and input trajectory is represented by $\bar{\zeta}(t)$ and $\bar{u}_0(t)$. Suppose the equivalent wrench of the load is determined by the feedback control law (33) and (34). The eigen-angle of the nominal rotation matrix of the load is represented by $\theta(t)$. The attitude control is determined by (23) and (25). If the positive constants k_1, k_2, k_3 and k_4 satisfy*

$$\begin{aligned}
&k_1 - \tfrac{1}{4\rho_1} > 0,\\
&k_2 \lambda(M_t)^{-1} - \rho_1 - \tfrac{1}{4\rho_2} - L_1 > 0,\\
&(\tfrac{1}{m_t}\cos\theta k_4 - \tfrac{k_3}{k_4} - \tfrac{L_2}{4\rho_1} - \tfrac{1}{4\rho_2}) > 0
\end{aligned}$$

then the state tracking error and the input of the closed loop system fall into the following sets,

$$\begin{aligned}
&e_{\tilde{R},0} \in \tilde{\Omega}_R = \{e_{\tilde{R},0} : \|e_{\tilde{R},0}\| \leq \sqrt{\tfrac{\rho_2}{\min(\beta_1,\beta_2)}} b_r := L_R\}\\
&\tilde{\omega}_0 \in \tilde{\Omega}_\omega = \{\tilde{\omega}_0 : \|\tilde{\omega}_0\| \leq (k_1+1)\sqrt{\tfrac{\rho_2}{\min(\beta_1,\beta_2)}} b_r\}\\
&\tilde{p}_{0,e} \in \tilde{\Omega}_p = \left\{\tilde{p}_{0,e} : \|\tilde{p}_{0,e}\| \leq \tfrac{k_4}{k_3}\sqrt{\tfrac{L_2\rho_3 L_R^2 + \rho_4 b_t^2}{\min(k_5,\beta_3)}}\right\}\\
&\tilde{v}_0 \in \tilde{\Omega}_v = \left\{\tilde{v}_0 : \|\tilde{v}_0\| \leq 2\sqrt{\tfrac{L_2\rho_3 L_R^2 + \rho_4 b_t^2}{\min(k_5,\beta_3)}}\right\}\\
&\tilde{\tau}_0 \in \tilde{\Omega}_\tau = \{\tilde{\tau}_0 : \|\tilde{\tau}_0\| \leq (\|M\|k_1(k_1+1) + L_3 k_1 + k_2)\\
&b_r\sqrt{\tfrac{\rho_2}{\min(\beta_1,\beta_2)}} := \Delta_\tau\Big\}\\
&\tilde{F}_0 \in \tilde{\Omega}_F = \left\{\tilde{F}_0 : \|\tilde{F}_0\| \leq k_4\sqrt{\tfrac{L_2\rho_3 L_R^2 + \rho_4 b_t^2}{\min(k_5,\beta_3)}} := \Delta_F\right\}
\end{aligned} \tag{41}$$

where $k_5 = \frac{k_3}{k_4}$, $L_R = \sqrt{\frac{\rho_2}{\min(\beta_1,\beta_2)}} b_r$, $\beta_1 = k_1 - \frac{1}{4\rho_1}$, $\beta_2 = k_2\lambda(M_t)^{-1} - \rho_1 - \frac{1}{4\rho_2} - L_1$, $\beta_3 = (\frac{1}{m_t}\cos\theta k_4 - k_5 - \frac{L_2}{4\rho_1} - \frac{1}{4\rho_2})$ *with positive constants ρ_1, ρ_2, ρ_3 and ρ_4, and $\lambda(M_t)$ is the minimum eigenvalue of M_t.*

Proof. See Appendix B in supplementary document. □

4. Main results

4.1. Outer loop tube-based MPC

Based on the nominal dynamics, nonlinear MPC (NMPC) is adopted to generate the nominal state and nominal input for (21) by considering the state and input constraints. The NMPC is typically solved at discrete time instants. Given the sampling time interval δ_t, the sampling time sequence $\{t_k\}$, $k \in \mathbb{N}$ can be generated. At a sampling time instant t_k, the NMPC is constructed by solving the following optimal control problem,

$$\begin{aligned}
&\min_{\bar{u}_0(s)} J(\bar{\zeta}, \bar{u}_0) = \quad V_r(\bar{\zeta}_r(t_k+\Gamma)) + V_t(\bar{\zeta}_t(t_k+\Gamma)) +\\
&\int_{t_k}^{t_k+\Gamma} \big(N_r(\bar{\zeta}_r(s), \bar{\tau}_0(s)) + N_t(\bar{\zeta}_t(s), \bar{F}_0(s))\big) ds\\
&s.t. \quad \dot{\bar{\zeta}}(s) = f(\bar{\zeta}, \bar{u}_0(s)),\\
&\bar{\zeta} \in \bar{\mathcal{X}} \times \bar{\mathcal{V}}, \bar{u}_0(s) \in \bar{U}, \bar{\zeta}(t_k+\Gamma) \in \Omega_r \times \Omega_t
\end{aligned} \tag{42}$$

where $\Gamma > \delta_t$ is the prediction horizon, $\zeta_r = (R_{0,e}, \omega_0)$ denotes the states of rotational motion, $\zeta_t = (p_{0,e}, v_0)$ is used to express the states of translational motion, $V_r(\bar{\zeta}_r)$ $V_t(\bar{\zeta}_t)$, $N_r(\bar{\zeta}_r, \bar{\tau}_0)$ and $N_t(\bar{\zeta}_t, \bar{F}_0)$ are positive definite functions that will be defined later, Ω_r and Ω_t are the terminal set that will be defined later, the admissible nominal wrench set $\bar{U}$ is defined as $\bar{U} = (S_5 \ominus \tilde{\Omega}_F) \times (S_7 \ominus \tilde{\Omega}_\tau)$, $\bar{\mathcal{X}}$ and $\bar{\mathcal{V}}$ are defined as,

$$\bar{\mathcal{X}} = \mathcal{X} \ominus (\tilde{\Omega}_R \times \tilde{\Omega}_p), \bar{\mathcal{V}} = \mathcal{V} \ominus (\tilde{\Omega}_\omega \times \tilde{\Omega}_v), \tag{43}$$

and $f(\bar{\zeta}, \bar{u}_0)$ is given by (21). Taking $\bar{S}_5 = S_5 \ominus \tilde{\Omega}_F$ and $\bar{S}_7 = S_7 \ominus \tilde{\Omega}_\tau$, $\bar{U}$ can thus be expressed from Lemma 1 and Proposition 2 as,

$$\bar{U} = \bar{S}_5 \times \bar{S}_7 \tag{44}$$

where $\bar{S}_5 = \{(\bar{F}_{0,x}, \bar{F}_{0,y}, \bar{F}_{0,z})^T : \bar{F}_{0,x}^2 + \bar{F}_{0,y}^2 \le (F_{m,h} - \Delta_F)^2 := \bar{F}_{m,h}^2, \Delta_F - F_{m,z} \le \bar{F}_{0,z} + m_t g \le F_{m,z} - \Delta_F\}, \bar{S}_7 = \{\tau_0 : \|\tau_0\| \le \tau_m - \Delta_\tau := \bar{\tau}_m\}$.

By solving (42), the nominal state trajectory $\bar{\zeta}(s|t_k)$ and the nominal control trajectory $\bar{u}_0(s|t_k)$ are therefore obtained. Given $\bar{\zeta}(s|t_k)$ and $\bar{u}_0(s|t_k)$, the equivalent wrench commands applied on the load $u_{0,d}(s|t_k)$ can then be obtained from the feedback control law (33) and (34).

From the desired thrust vector of the aerial vehicle, there are several ways to transform the thrust vector into the attitude and thrust magnitude of the vehicle. The thrust magnitude of the aerial vehicle can be obtained directly from the norm of the thrust vector as,

$$T_i = \|\Upsilon_i\| \tag{45}$$

Given the yaw angle reference trajectory $\bar{\psi}(t)$, the reference attitude trajectory can be calculated as,

$$\begin{aligned} \bar{R}_i e_3 &= -\tfrac{1}{T_i} R_0 \Upsilon_i \\ \bar{R}_i e_2 &= (\cos(\bar{\psi}(t)), \sin(\bar{\psi}), 0) \times \bar{R}_i e_3 \\ \bar{R}_i e_1 &= \bar{R}_i e_2 \times \bar{R}_i e_3 \end{aligned} \tag{46}$$

4.2. Terminal control of the nominal dynamics

In order to prove the feasibility and convergence of the nominal closed loop system with nominal MPC, we will first consider the terminal control for the nominal dynamics on the time interval $[t_k + \Gamma, t_{k+1} + \Gamma]$. The terminal control will be designed and analyzed in two steps. In first step, the terminal control of rotational part of the nominal load dynamics will be considered. Then, the terminal control of the translational part of the nominal load dynamics will be considered.

4.2.1. Terminal control for rotational motion

For the nominal rotational motion of the load, design the commanded angular velocity as,

$$\bar{\omega}_{0,d} = -k_6 \bar{e}_{R,0} \tag{47}$$

where k_6 is a positive constant, and $\bar{e}_{R,0} = \frac{1}{2}(\bar{R}_{0,e} - \bar{R}_{0,e}^T)^\vee$.

From (47) we further design the terminal control low for $\bar{\tau}_0$ as,

$$\bar{\tau}_0 = -k_7 M_t \bar{\omega}_{0,e} + \bar{\omega}_0 \times M_t \bar{\omega}_0 + M_t \dot{\bar{\omega}}_{0,d} \tag{48}$$

where k_7 is a positive constant, and $\bar{\omega}_{0,e} = (\bar{\omega}_0 - \bar{\omega}_{0,d})$.

Substituting (48) into the nominal EOM (21) yields,

$$\dot{\bar{\omega}}_{0,e} = -k_7 \bar{\omega}_{0,e} \tag{49}$$

Taking $\bar{\zeta}_r = (\bar{e}_{R,0}^T, \bar{\omega}_0^T)^T$ and $\bar{\xi}_r = (\bar{e}_{R,0}^T, \bar{\omega}_{0,e}^T)^T$, it is concluded that

$$\bar{\xi}_r = \begin{bmatrix} I & 0 \\ k_6 I & I \end{bmatrix} \bar{\zeta}_r := A_r \bar{\zeta}_r \tag{50}$$

Then we have the following proposition which is necessary for the feasibility and convergence analysis of the entire system.

Proposition 3. *Consider the nominal rotational EOM of the load, define a set* $\Omega_r = \{\bar{\zeta}_r : V_r(\bar{\zeta}_r) = \frac{1}{2} tr(I - \bar{R}_{0,e}) + \frac{1}{2} h_{11} \|\bar{\omega}_0 + k_6 \bar{e}_{R,0}\|^2 \le \epsilon_r := \frac{\bar{\tau}_m^2}{\max\left(\frac{l_9}{2}, \frac{2 l_8}{h_{11}}\right)}\}$, *where* h_{11} *is a positive constant. If* $\bar{\zeta}_r(t_k + \Gamma) \in \Omega_r$, *the control law* $\bar{\tau}_0(s), s \in (t_k + \Gamma, t_{k+1} + \Gamma)]$ *is given by (47) and (48), where the parameters are appropriately selected, then the following propositions hold for all* $s \in (t_k + \Gamma, t_{k+1} + \Gamma)]$,

1) Ω_r *is an invariant set,*

2) $\dot{V}_r + N_r(\bar{\zeta}_r, \bar{\tau}_0) \le 0$, *where*

$$\begin{aligned} N_r &= \bar{\zeta}_r^T A_r^T \begin{bmatrix} q_{11} I & 0 \\ 0 & q_{12} I \end{bmatrix} A_r \bar{\zeta}_r + \bar{\tau}_0^T r_1 \bar{\tau}_0 \\ &:= \bar{\zeta}_r^T Q_r \bar{\zeta}_r + \bar{\tau}_0^T R_r \bar{\tau}_0 \end{aligned}$$

with positive constants q_{11}, q_{12} *and* r_1.

3) $\bar{\tau}_0 \in \bar{S}_7$ *for all* $\bar{\zeta}_r \in \Omega_r$.

Proof. See Appendix C in the supplementary document. □

4.2.2. Terminal control for translational motion

For the nominal translational motion of the load, we design the commanded velocity as,

$$\bar{v}_{0,d} = -k_8 \bar{p}_{0,e} \tag{51}$$

where k_8 is a positive constant.

From (51) we further design the feedback control low for $\bar{F}_0$ as,

$$\bar{F}_0 = -k_9 m_t \bar{R}_0^T \bar{v}_{0,e} - \bar{R}_0^T m_t g e_3 + \bar{R}_0^T m_t \dot{\bar{v}}_{0,d} \tag{52}$$

where k_9 is a positive constant, and $\bar{v}_{0,e} = \bar{v}_0 - \bar{v}_{0,d}$.

For the translational motion of the load, we express $\bar{\zeta}_t = (\bar{p}_{0,e}^T, \bar{v}_0^T)^T$ and $\bar{\xi}_t = (\bar{p}_{0,e}^T, \bar{v}_{0,e}^T)^T$. Then it is concluded that

$$\bar{\xi}_t = \begin{bmatrix} I & 0 \\ k_8 I & I \end{bmatrix} \bar{\zeta}_t := A_t \bar{\zeta}_t \tag{53}$$

We have the following proposition which is necessary for the feasibility and convergence analysis.

Proposition 4. *Consider the nominal translational EOM of the load, the nominal attitude of the load satisfies $e_3^T \bar{R}_0 e_3 \geq L_l$, where $L_l < 1$ is a positive constant. Define a set $\Omega_t = \{\bar{\zeta}_t : V_t(\bar{\zeta}_t) := \frac{1}{2}\bar{\zeta}_t^T H_t \bar{\zeta}_t \leq \epsilon_t^2\}$, where H_t is a positive definite matrix defined from*

$$H_t = A_t^T \begin{bmatrix} h_{21} I & 0 \\ 0 & h_{22} I \end{bmatrix} A_t$$

with positive constants h_{21} and h_{22}, and

$$\epsilon_t = \min \left(\frac{F_{m,z} - \Delta_F}{\sqrt{2} m_t (\frac{k_8 + k_9}{\sqrt{h_{21}}} + \frac{k_8^2}{\sqrt{h_{22}}})}, \frac{\bar{F}_{m,h} - m_t g \sqrt{1 - L_l^2}}{\sqrt{2} m_t (\frac{k_8 + k_9}{\sqrt{h_{11}}} + \frac{k_8^2}{\sqrt{h_{22}}})} \right)$$

If $\bar{\zeta}_t(t_k + \Gamma) \in \Omega_t$, the control law $\bar{F}_0(s), s \in (t_k + \Gamma, t_{k+1} + \Gamma)]$ is given by (51) and (52), where the parameters are appropriately selected, then the following propositions hold for all $s \in (t_k + \Gamma, t_{k+1} + \Gamma)]$,

1) Ω_t is an invariant set,

2) $\dot{V}_t + N_t \leq 0$, where

$$N_t = \bar{\zeta}_t^T A_t^T \begin{bmatrix} q_{21} I & 0 \\ 0 & q_{22} I \end{bmatrix} A_t \bar{\zeta}_t + (\bar{F}_0 + m_t \bar{R}_0^T g e_3)^T r_2 (\bar{F}_0 + m_t \bar{R}_0^T g e_3)$$

with positive constants q_{21}, q_{22} and r_2.

3) $\bar{F}_0 \in \bar{S}_5$ for all $\bar{\zeta}_t \in \Omega_t$.

Proof. See Appendix D in supplementary document. □

4.3. Feasibility and stability of the overall system

Theorem 1. *Consider the MAVTS (6). The nominal state $\bar{\zeta}$ and nominal wrench $\bar{u}_0$ is solved from the nominal finite time optimal problem (42). The feedback control law for the equivalent wrench $u_{0,d}$ is determined by (33) and (34). The attitude control of each aerial vehicle is determined by (25). Suppose that at initial time instant the finite time optimal problem is feasible. Then the closed loop system is input-to-state stable (ISS) with respect to the disturbances.*

Proof. See Appendix E in supplementary document. □

4.4. Algorithm synthesis

From the results of Theorem 1, the algorithm of implementing the tube-based MPC for the entire system is shown in Algorithm 1. We can therefore conclude that such an algorithm can force the system to achieve ISS with respect to the disturbance. While the tracking error of the actual system is always kept in an invariant set along the nominal trajectory, and the input to each aircraft always falls into the admissible input sets. Problem 1 is thus solved.

Remark 2. From Theorem 1, the obtained commanded equivalent wrench $u_{0,d}$ always falls in the admissible set $\bar{U}$. This means that the allocation solution $\bar{R}_i$ and T_i from $u_{0,d}$ always satisfies the constraints. For brevity, the detailed allocation procedure is omitted in this article.

Algorithm 1 Synthesis of the algorithm.

Initialization: At time instant t_0, let $\zeta(0) = \bar{\zeta}(0)$.

1: At time instant t_k, solve the nominal MPC problem, obtain the nominal equivalent wrench input $\bar{u}_0(s), s \in [t_k, t_k + \Gamma)$.
2: **for all** $s \in [t_k, t_{k+1})$ **do**
3: Using (33) and (34), obtain the commanded equivalent wrench $u_{0,d}(s)$.
4: Compute the commanded attitude $\bar{R}_i(s)$ and thrust $T_i(s)$ of each aerial vehicle from $u_{0,d}(s)$.
5: Using (25), obtain the commanded torque $\tau_i(s)$ of each aerial vehicle.
6: Apply the actual control input $\tau_i(s)$ and $T_i(s)$ to each aerial vehicle.
7: **end for**
8: $\left(\zeta(t_k), \bar{\zeta}(t_k)\right) \leftarrow \left(\zeta(t_{k+1}), \bar{\zeta}(t_{k+1})\right)$, $t_k \leftarrow t_{k+1}$.
9: Go to step 1.

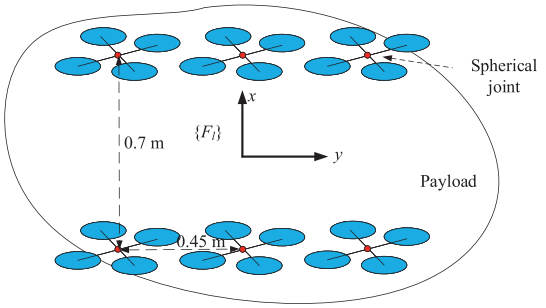

Fig. 6. The location of the multiple aerial vehicles in the simulation.

Table 2
Physical parameters of the quadrotor aerial vehicle.

Parameters	Value
Location of quadrotors in $\{F_I\}$	$(0.35, 0, 0)$m, $(0.35, -0.45, 0)$m, $(-0.35, -0.45, 0)$m $(-0.35, 0, 0)$m, $(-0.35, 0.45, 0)$m, $(0.35, 0.45, 0)$m
Mass of each quadrotor	1.121 kg
Inertia tensor of each quadrotor	diag (0.01, 0.0082, 0.0148) $kg \cdot m^2$
Thrust coefficient of propellers	$1.2953 \times 10^{-5} N/(rad/s)^2$
Drag coefficient of propellers	$1.0368 \times 10^{-7} Nm/(rad/s)^2$
Mass of the load	5 kg

5. Simulation and discussion on real-world implementation

5.1. Numerical simulation

5.1.1. Simulation scenarios

In the numerical simulation, 6 quadrotor vehicles are considered to provide the thrust for the transportation system. The location of the quadrotor in $\{F_I\}$ is shown in Fig. 6, and is summarized in Table 2. The physical parameters of each quadrotor are selected from a real quadrotor, as seen in Table 1 in [38], and are summarized in Table 2 in this paper. The thrust coefficient and drag coefficient of the propellers are selected from [39].

In the simulation, the flapping effect and the actuator dynamics for the propellers are also considered. The modeling of the flapping effect is borrowed from [39]. The flapping effect of the rotors make the thrust not strictly in line with the z-axis of the body frame.

Besides, the actuator dynamics of the rotors is modeled as a first-order plus time delay system [40],

$$G(s) = \frac{1}{1 + T_a s} e^{-\tau_a s}$$

where T_a is the time constant, and τ_a is the time delay. In [40], it is seen that $T_a = 0.041$, and $\tau_a = 0.0015$ for a 12-inch rotor.

The initial configuration of the load is:

$$p_0(0) = (2 + z_1, z_2, 10 + z_3)\text{m}, R_0(0) = \exp\left(\hat{z}_4\right) \exp\left(0.4(1, 1, 0)\right)^{\hat{}}$$

where z_1, z_2 and z_3 are random numbers between 0 and 1, and $z_4 \in S^2$ is the random vector.

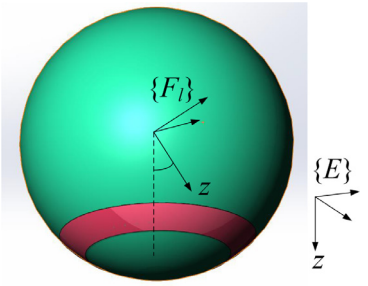

Fig. 7. The illustration of the attitude constraint of the load in the simulation. This means that the angle between the z axis of $\{E\}$ and $\{F_l\}$ should be in the range of $[\cos^{-1}(0.85), \cos^{-1}(0.7)]$, i.e., the z axis of $\{F_l\}$ should point to the red belt in this figure.

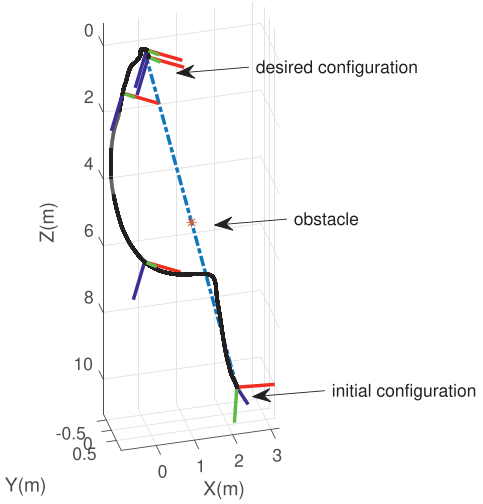

Fig. 8. The configuration trajectory of the load. (Red: R_0e_1, green: R_0e_2, blue: R_0e_3.) .

And the desired configuration of the load is

$$p_{0,d} = (0,0,0)\text{m}, R_{0,d} = \exp\left(-0.6(\frac{1}{\sqrt{2}}, \frac{1}{\sqrt{2}}, 0)\right)^{\wedge}$$

The illustration of an example of the initial and desired configuration can be seen in Fig. 8.

In the simulation, we also test different time constant T_a with 0.021, 0.041, 0.051, 0.061 and 0.07. For each different T_a, we run 50 test trials with the following conditions, and check the test data to see if the system is stable, and if the constraints are fulfilled.

- The random disturbance acting on the aircraft is given by $d_i \sim U(-1,1)$. The disturbance acting on the load is given by $d_{0,t} \sim U(-1,1)$ and $d_{0,i} \sim U(-1,1)$.
- An obstacle with radius of 1.5 m is set at the position of $\frac{p_0(0)}{2}$. The MAVTS should keep away from the obstacle. It is noted that the obstacle is on the straight way from the initial position to the desired position.
- The constraint on the attitude of the load is set as $0.8 \le e_3^T R_0 e_3 \le 0.85$. The physical meaning of such constraint is illustrated in Fig. 7.
- The constraint on the spherical joint connecting to each quadrotor is $e_3^T R_0^T R_i e_3 \ge 0.7$.
- The wrench acting on the system generated by the system is projected into the admissible set $S_5 = \{F_0 : F_{0,x}^2 + F_{0,y}^2 \le (35N)^2, \|F_{0,z} + m_t g\| \le 42N\}, S_7 = \{\tau_0 : \|\tau_0\| \le 15.2N \cdot m\}$, which are calculated according to thrust-weight ratio of each quadrotor.
- We restrict the angular velocity of the load by adding the constraint $\|\omega_0\| < 1\text{rad/s}$.

According to the physical parameters and the equation of motion of the MAVTS, the Lipchitz constants in (36) and (39) are calculated as $L_1 = 1.363$ and $L_3 = 2.0936$. The constant L_2 is set to 3 considering the thrust-weight ratio of each quadrotor. The open source ACADO is used to solve the NMPC problem in the outer loop control [41]. In solving the optimal control problem (42), the prediction horizon is set to 0.7 s, and the sampling time is 0.1 s.

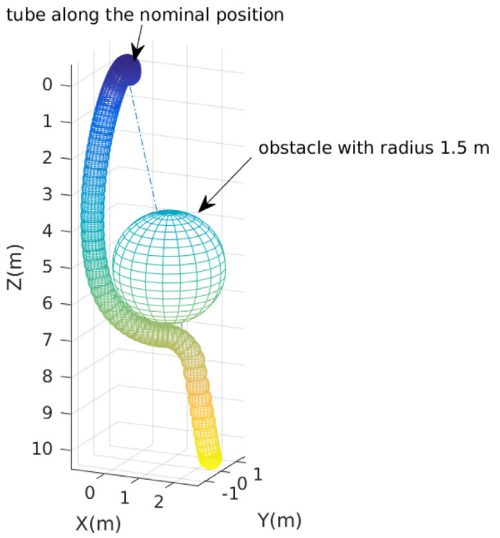

Fig. 9. The tube along the nominal position. The tube is 0.3033 m calculated from Proposition 2. The actual position keeps inside the tube. The tube should not interact with the obstacle so as to ensure the geometric safety.

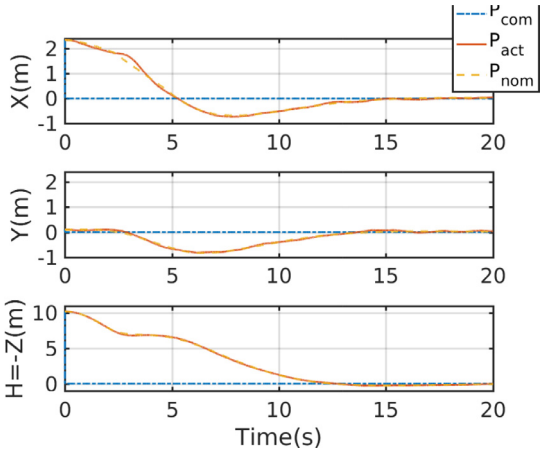

Fig. 10. The position evolution of the load. The virtual line represents the desired position, the solid line represents the actual position, and the dot-dash line represents the nominal position generated by the nominal MPC.

5.1.2. Results

In the simulation we found that if the time constant T_a is greater than 0.07, the system becomes unstable. While if the system is stable, the simulation results show that the constraints are all fulfilled.

When $T_a = 0.041$, one set of the simulation results is shown in Figs. 8 - 16. From Proposition 2 and the upper bound of the disturbances, we can calculate the upper bound of the attitude tracking error and the position tracking error as $\|e_{\tilde{R}_0}\| \leq 0.1563$ and $\|\tilde{p}_{e,0}\| \leq 0.3033$m. The tube along the nominal position trajectory is shown in Fig. 9, where it is seen that the actual position trajectory always locates inside the tube. By considering the tube along the nominal position trajectory, the obstacle in the nominal MPC is revised into 1.8033 m. The position of the load is depicted in Figs. 8 - 10. It is seen that the nominal MPC generates the nominal trajectory of the load from the initial configuration to the desired configuration, while keeping the position constraint satisfied. The geometric safety in terms of the obstacle avoidance is thus achieved. The load's attitude evolution from initial attitude to the goal attitude is depicted in Fig. 11, while the attitude error of the load defined by $\|R_0 - \bar{R}_0\|$ is shown in Fig. 12. It is seen that the attitude error is bounded in the presence of disturbance and uncertainties. The fulfilled position and attitude constraints are shown in Figs. 13 - 14.

During the simulation, the attitude of each aerial vehicle is varying at all the time. This means that the direction of the multiple thrust is also varying. As an example, the commanded attitude of the first vehicle is shown in Fig. 15, and the attitude tracking error of the first vehicle is shown in Fig. 16. It is seen that the attitude tracking error of this quadrotor is also bounded. As the equivalent wrench output from the tube-based MPC is admissible, the transformed attitude of each

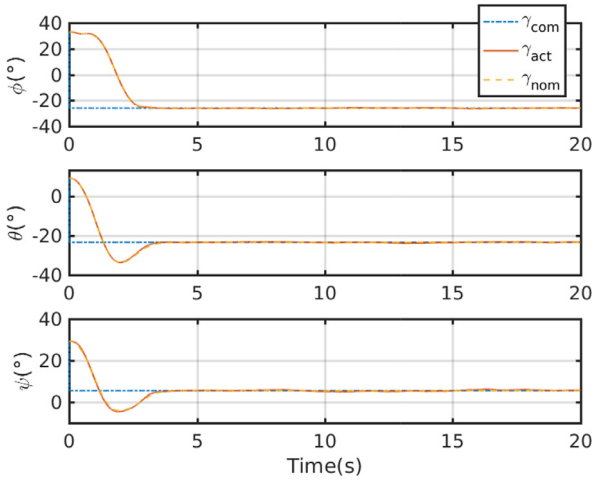

Fig. 11. The attitude evolution of the load.

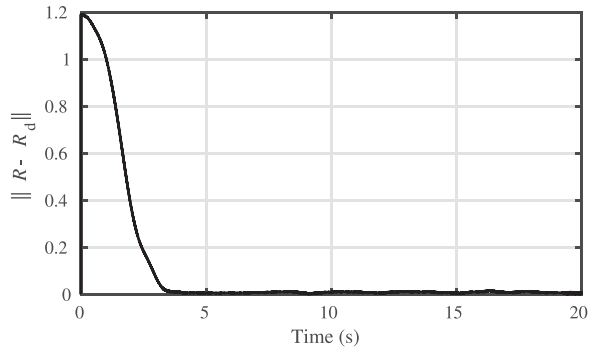

Fig. 12. The attitude error of the load.

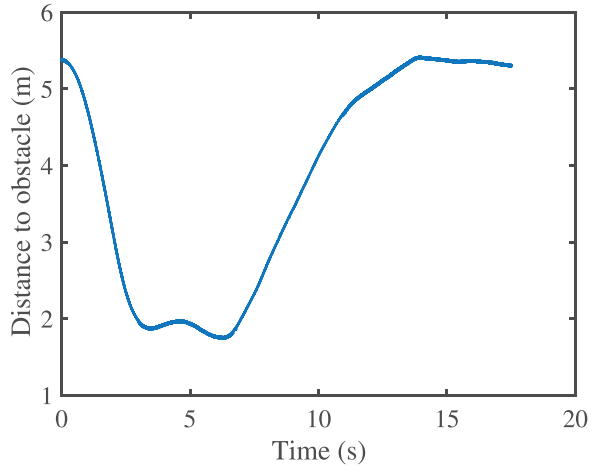

Fig. 13. The position constraint expressed by the distance from the obstacle.

quadrotor is also in the admissible set. The thrust magnitude of each quadrotor is shown in Fig. 17, which shows that the thrust magnitude of each quadrotor is always less that $L_2 m_i g$, thus is in the admissible input set.

Remark 3. As indicated in Problem 1, we need the load to be transported from the initial pose to the desired pose, while to fulfill the constraints in the presence of uncertainties and input boundedness. The initial configuration and the desired configuration should be in the admissible state set. Otherwise, the tube-based MPC is not feasible, then as seen from Theorem 1, the system cannot be guaranteed stable. If the simulation scenarios are not in line with the conditions of Theorem 1, e.g.,

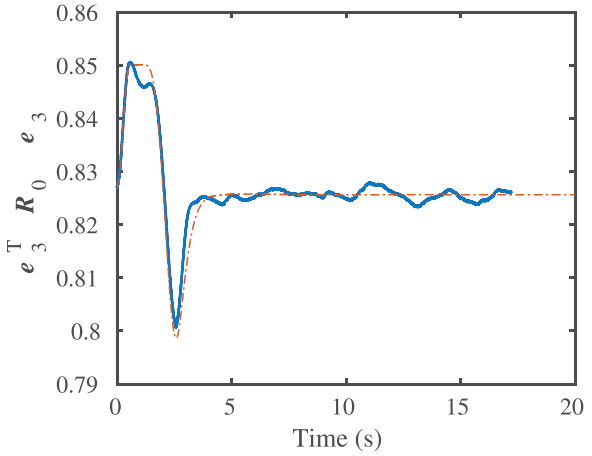

Fig. 14. The attitude constraint on the load.

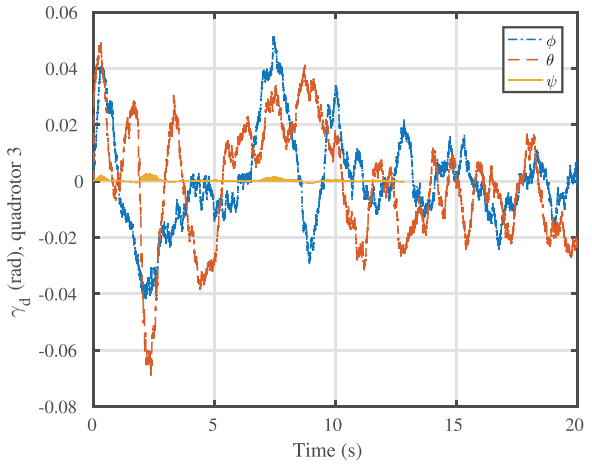

Fig. 15. The commanded attitude of quadrotor 1, expressed in Euler angles.

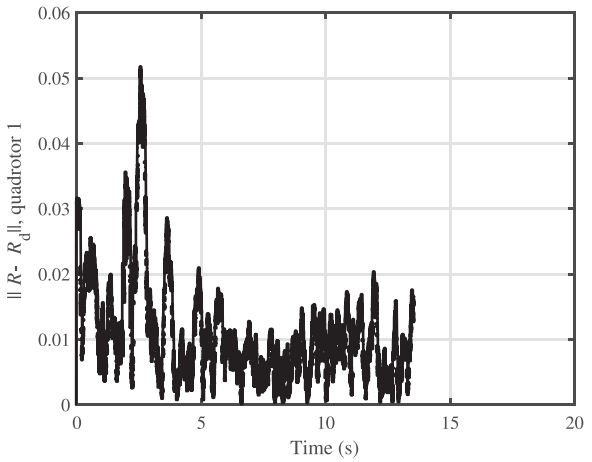

Fig. 16. The attitude tracking error of quadrotor 1.

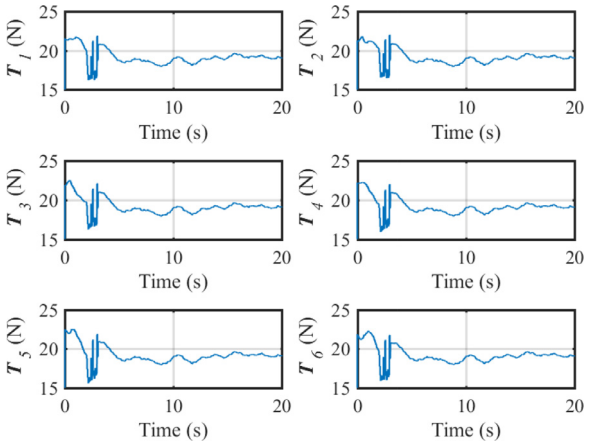

Fig. 17. The thrust magnitude of each quadrotor.

the initial configuration and the desired configuration does not fall into the admissible set, then the system may not be stabilized. This is why the initial configuration and the desired configuration are designed as seen in the simulation scenario. Besides, the feedback control parameters should be appropriately selected according to Proposition 2 to keep the system stable.

Remark 4. The ISS of the system means that the magnitude of the regular perturbation does not influence stability of the system. Propositions 3 and 4 show that the tube of the tracking error is proportional to the disturbance magnitude. The tube is then used to revise the admissible state and input set in the nominal MPC. The larger is the magnitude of the tube, the smaller the admissible state and input set in the nominal MPC are. By considering the tube, the safety of the system is enhanced, but at the same time, the system response becomes conservative. Conservative estimation of the disturbance may make the nominal trajectory generated by the nominal MPC become conservative, e.g., too far away from the obstacle in the obstacle avoidance problem.

Remark 5. In the simulation, the actuator dynamics is also considered in the system. Such actuator dynamics induces the singular perturbation in the system, and is not analyzed in the proof. The singular perturbation theorem may be adopted to analyze the stability of the entire system considering actuator dynamics. In this paper, the simulation is used to demonstrate the effect of actuator dynamics. Under the conditions listed in the simulation, when the time constant is greater than a threshold, the system becomes unstable. This implies that the actuator dynamics should be fast enough. This is a factor that may affect the stability in real-world systems, and should be considered in the prototype design and implementation.

5.2. Comparison

As a comparison, we adopted a baseline controller for the system to transport the load from initial pose to the desired pose. In the comparison simulation, the parameters, disturbance, and constraints of the system are all the same as in the previous simulation case. The controller is adopted from (24)-(31) in [42]. The results with well-tuned controller gains are shown in Figs. 18 - 20. It is noted that the desired pose of the load is different from the initial pose of the load at the initial instant, i.e., there is large initial error. While there are uncertainties, state and input constraints in the system. Under such conditions, the baseline controller is also able to let the load arrive at the desired pose from the initial pose. However, it is seen that the baseline controller is not able to deal with the state and input constraints *online*. Therefore, the obstacles are not avoided by the MAVTS in this simulation case, as seen in Fig. 18 and Fig. 20. The position trajectory interacts with the obstacles in the comparison simulation. Moreover, there is large overshoot in the position tracking of the load in the comparison case. This is partly induced by the fact that the baseline controller is unable to fulfill the input constraints, it may produce control input outside of the admissible input set. While input itself is indeed bounded in the plant of the simulation. This induces additional input disturbances. Therefore, the tracking error may become large and may make overshoot in the comparison simulation. Through the comparison simulation, the capability of our proposed methodology to fulfill the state constraints under bounded input and uncertainties is further verified.

5.3. Hardware-in-the-loop simulation and discussion on real-world implementation

In order to explore the real-time performance of the presented algorithm in real-world system, a middle-ware of the real-time MAVTS prototype is developed. We implemented the real-time hardware-in-the-loop (HIL) simulation based on the developed middle-ware.

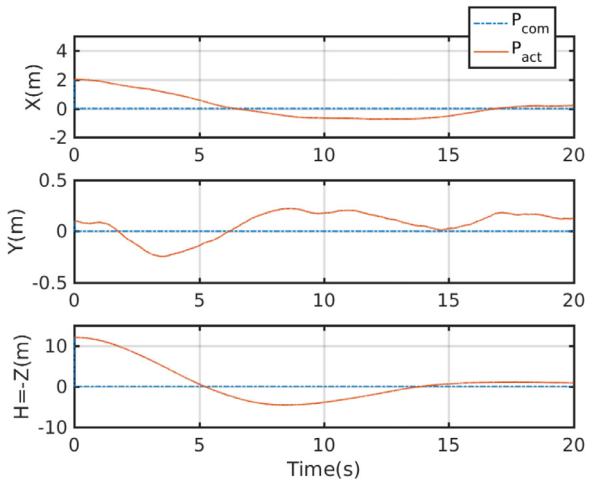

Fig. 18. The position evolution of the load, in the comparison simulation.

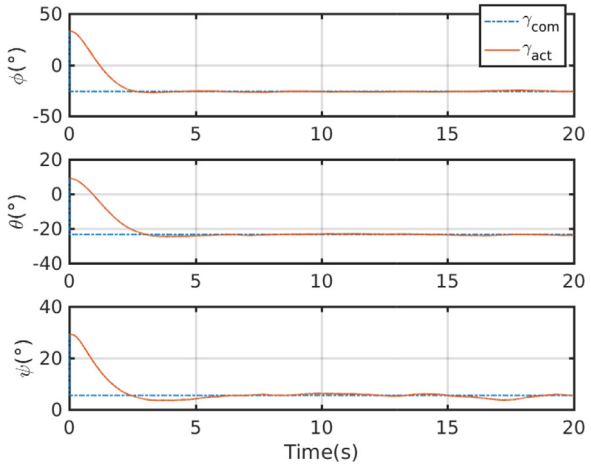

Fig. 19. The attitude evolution of the load, in the comparison simulation.

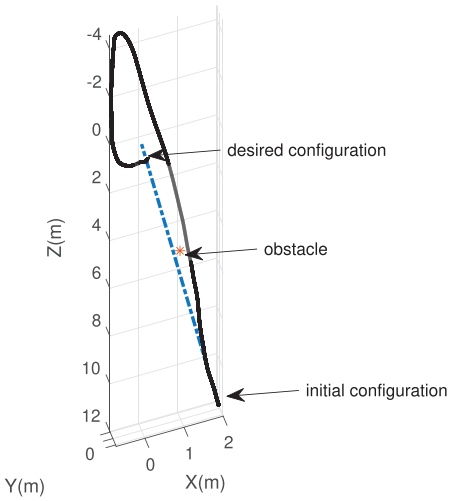

Fig. 20. The 3D position of the load, in the comparison simulation.

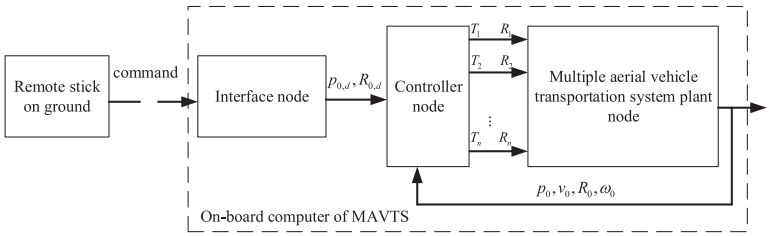

Fig. 21. The architecture of real-time simulation system of the MAVTS in ROS.

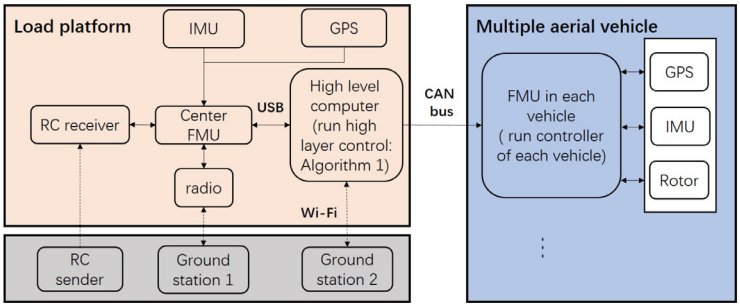

Fig. 22. The hardware architecture of the MAVTS prototype.

5.3.1. Hardware-in-the-loop simulation

In implementing the real-world system, the outer loop of the tube-based MPC is developed in C++ and Ubuntu 18.04/ROS software environment [43]. The ROS framework supports the multi-thread programming. Each thread of the program is called a ROS node [43]. Based on (6), (10) and (11), the ROS nodes of the simulated MAVTS plant are developed. To simulate the real-world flight, uncertain disturbance is added to the plant as in Section 5.1. The remaining ROS nodes in the simulation act as the interfaces which receive commanded signals from the remote-control stick and convert the signals into the reference position and attitude. The architecture of the real-time simulation system is shown in Fig. 21. By adopting the ROS framework, such a real-time simulation system can be easily transplanted to the real-world system. The NMPC in the outer loop is also solved with the ACADO solver. Different from the simulation in MATLAB, in the hardware-in-the-loop simulation, the ACADO with C++ interfaces is adopted.

In the real-world system, the HIL simulation is conducted. We also carefully designed the modes and the switches of the controller in the HIL simulation to let the system can switch among different modes such as take-off, flight and landing. The HIL simulation results show that the developed middle-ware of the proposed control scheme on the hardware system can satisfy the real-time requirements, therefore is suitable for implementation.

5.3.2. Discussion on real-world implementation

Each aerial vehicle used in the prototype is a self-developed small-scale quadrotor drone, which also contains a complete set of avionics equipment. Therefore, each aerial vehicle can fly individually. The flight control of each aerial vehicle is constructed based on the PX4 open-source flight controller.

To satisfy the requirements of reliability and real-time communication among multiple sub-aircraft, the CAN bus is used to construct the reliability, extendable, and real-time communication among multiple vehicles in the prototype. The high level computer and the flight control modules of each vehicle are considered as nodes mounted on the CAN bus. Unlike the common wireless communication in aerial vehicle swarms, such a bus-based wired communication system not only satisfies the reliability and real-time communication, but also allows expansion of the quantity of vehicles. The architecture of the developed hardware system is shown in Fig. 22.

Based on the designed hardware system, the software of the MAVTS prototype is developed in ROS framework. The controller scheme Algorithm 1 run as ROS nodes are installed on the high level computer mounted on the load platform. Meanwhile, a one-to-many communication protocol, *Swarmlink*, is designed for the MAVTS, with corresponding decoding and encoding nodes on both payload platform and sub-aircraft. The overall system software architecture is shown in Fig. 23. As shown in the figure, the *Decision* node is used to receive the remote control commands, and transmit the commands to the position and attitude controller. The *Controller* node is implemented from the outer loop tube-based MPC in C++. The *Swarmlink* node encodes and publishes the communication data packets on the CAN bus according to the *Swarmlink* protocol. It also decodes the data packets received from the CAN bus and converts them into the data packets with other format that can be subscribed by other ROS nodes on the high level computer. Based on the developed MAVTS prototype composed of three quadrotor aerial vehicles, preliminary flight is performed.

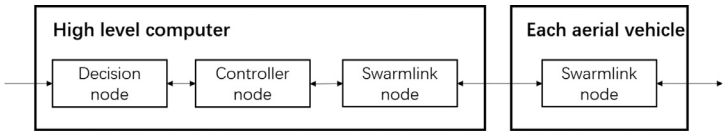

Fig. 23. The software architecture based on ROS implemented in the MAVTS prototype.

Remark 6. It is noted that to apply the complete control scheme in the real-world system, we need the information of the upper bound of the disturbance. As seen in the proof of Theorem 1, the upper bound of the disturbance can be used to revise the admissible state and input set in the nominal MPC, thus ensure the safety of the system. The bounded disturbance can be identified by comparing the experimental data from a test vehicle and the state prediction from model (6). By measuring and recording the actual states from the real vehicle and the nominal state predicted from the nominal model, the bounded information can be obtained [20]. It is noted that the model mismatch and disturbance identification is not the focus of this paper. Accurate estimation of the upper bound of the disturbance also needs plenty of real-world data. However, it is also noted that even if the estimation is conservative and is not accurate enough, it does not influence the stability of the system.

6. Conclusions

In this paper, the control problem of the multiple aerial vehicle transportation system has been considered. The 6D pose of the load can be adjusted separately because the multiple vehicles can provide thrust with different directions. As the multiple aerial vehicle transportation system is a highly complex system, a controller with a hierarchical structure has been designed to simplify the design procedure. Different from other work, the admissible state and input set in the tube-based model predictive control of this paper is revised considering the attitude tracking error of the lower layer-controlled subsystem, therefore the safety of the higher layer system is guaranteed. To the best knowledge of the authors, this is the first time that the tube-based model predictive control is applied to the multiple aerial vehicle transportation system. The mathematical proof and the simulation results have shown that the proposed control approach can efficiently deal with the state/input constraints and uncertainties. In addition, it is mentioned that the attitude tracking error of the system is expressed by rotation matrix directly, therefore the singularity problem and unwinding problem due to the local expression of attitude has been avoided in our work. The hardware-in-the loop simulation and the preliminary flight results demonstrate that the overall proposed control scheme is suitable for real-world system.

Acknowledgments

This work was supported by the National Natural Science Foundation of China (NSFC) [grant number 62173037]; the HYFLIERS project [grant number 779411]; the AERIAL-CORE project [grant number 871479]; and State Key Laboratory of Robotics and Systems (HIT) [grant number SKLRS-2022-KF-07].

Appendix A.

Appendix B. Proof of proposition 1

Proof. Define the Lyapunov candidate for quadrotor attitude dynamics as,

$$V_1 = \frac{1}{2}\tilde{\omega}_i^T\tilde{\omega}_i + \frac{1}{2}\kappa_1\tilde{b}_a^2 \tag{A.1}$$

Differentiating V_1 along the trajectory of (11) yields,

$$\begin{aligned}\dot{V}_1 &= \tilde{\omega}_i^T\dot{\tilde{\omega}}_i - \kappa_1\tilde{b}_a\dot{b}_a^* \\ &= \tilde{\omega}_i^T\left[-k_{i,2}\tilde{\omega}_i - b_a^*\tanh\left(\frac{\tilde{\omega}_i}{\epsilon_1}\right) + d_i\right] - \kappa_1\tilde{b}_a\dot{b}_a^*\end{aligned} \tag{A.2}$$

Substituting (26) into (A.2) we have,

$$\dot{V}_1 \le -\tilde{\omega}_i^T k_{i,2}\tilde{\omega}_i + b_a\|\tilde{\omega}_i\| - \tilde{\omega}_i^T b_a\tanh\left(\frac{\tilde{\omega}_i}{\epsilon_1}\right) + \kappa_1\gamma_1 b_a^*\tilde{b}_a \tag{A.3}$$

From Lemma 2, we have

$$b_a\|\tilde{\omega}_i\| \le b_a\left(\tilde{\omega}_i^T\tanh\left(\frac{\tilde{\omega}_i}{\epsilon_1}\right) + k_t\epsilon_1\right) \tag{A.4}$$

Combining (A.4) and (A.3) yields,

$$\dot{V}_1 \leq -k_{i,2}\|\tilde{\omega}_i\|^2 + b_a k_t \epsilon + \kappa_1\gamma_1 b_a^* \tilde{b}_a \tag{A.5}$$

Moreover, from Young's inequality, given a positive constant $\delta > \frac{1}{2}$ we have,

$$b_a^*\tilde{b}_a = b_a\tilde{b}_a - \tilde{b}_a^2 \leq \frac{1}{2\delta}\tilde{b}_a^2 + \frac{\delta}{2}b_a^2 - \tilde{b}_a^2 = -\frac{2\delta-1}{2\delta}\tilde{b}_a^2 + \frac{\delta}{2}b_a^2 \tag{A.6}$$

Then (A.5) can be expressed as,

$$\dot{V}_1 \leq -k_{i,3}\|\tilde{\omega}_i\|^2 + k_t\epsilon_1 b_a - \kappa_1\gamma_1\tfrac{2\delta-1}{2\delta}\tilde{b}_a^2 + \tfrac{\delta\kappa_1\gamma_1}{2}b_a^2 \tag{A.7}$$

For the outer loop of the control, we consider the following Lyapunov function candidate,

$$V_2(R_i) = \frac{1}{2}\operatorname{tr}(I - \tilde{R}_i^T R_i) \tag{A.8}$$

which is a function of attitude error and is valid on $\{R_i : \operatorname{tr}(\tilde{R}_i^T R_i) < 2\}$.

Expanding $\tilde{R}^T R$ in (A.8) with Rodrigues' formula, we have,

$$V_2 = \frac{1}{2}\operatorname{tr}\left(-\sin(\|a\|)\frac{\hat{a}}{\|a\|} - \frac{\hat{a}^2}{\|a\|^2}[1-\cos(\|a\|)]\right) \tag{A.9}$$

where $a \in \mathbb{R}^3$. It is seen $\operatorname{tr}\left(\sin(\|a\|)\frac{\hat{a}}{\|a\|}\right) = 0$, $\operatorname{tr}(\hat{a}^2) = -2\|a\|^2$, therefore,

$$V_2 = 1 - \cos(\|a\|) \tag{A.10}$$

It is natural to verity that,

$$\dot{V}_2 = e_{R,i}^T E_{\omega,i} \tag{A.11}$$

where $E_{\omega,i} = \omega_i - (\tilde{R}_i^T\dot{\tilde{R}}_i)^\vee$.

Finally, define the following Lyapunov function candidate for the rotational motion of each aerial vehicle as,

$$V_a = V_1 + V_2 \tag{A.12}$$

Combining (A.7) and (A.11), we can obtain the derivative of V_a as

$$\dot{V}_a = e_{R,i}^T(-k_{i,1}e_{R,i} + \tilde{\omega}_i) + \dot{V}_1 \tag{A.13}$$

Applying Young's inequality, we have,

$$e_{R,i}^T\tilde{\omega}_i \leq \frac{1}{2}e_{R,i}^2 + \frac{1}{2}\tilde{\omega}_i^2 \tag{A.14}$$

Substituting (A.14) and (A.7) into (A.13), we can rewrite the expression of $\dot{V}_a$ as,

$$\begin{aligned}\dot{V}_a \leq & -\left(k_{i,1} - \tfrac{1}{2}\right)\|e_{R,i}\|^2 - \left(k_{i,2} - \tfrac{1}{2}\right)\|\tilde{\omega}_i\|^2 - \\ & \left(\kappa_1\gamma_1\tfrac{2\delta-1}{2\delta}\right)\tilde{b}_a^2 + C_1\end{aligned} \tag{A.15}$$

where $C_1 = k_t\epsilon b_a + \frac{\delta\kappa_1\gamma_1}{2}b_a^2$.

If we appropriately select parameters $k_{i,1}$, $k_{i,2}$, κ_1 and γ_1, we can further express $\dot{V}_a$ as,

$$\dot{V}_a \leq -C_2 V_a + C_1 \tag{A.16}$$

where C_2 is positive constant. Then we can conclude that

$e_a \leq 2\sqrt{\frac{C_1}{C_2}}$, where $e_a \in \{\|e_{R,i}\|, \|\tilde{\omega}_i\|, \|\tilde{b}_a\|\}$. This completes the proof. □

Appendix C. Proof of Proposition 2

Proof. We define the following Lyapunov candidate for the rotational part of (30),

$$V_{l1} = \operatorname{tr}(I - \tilde{R}_{0,e}^T R_{0,e}) + \frac{1}{2}e_{\omega,0}^T e_{\omega,0} \tag{B.1}$$

which is positive definite.

From (35), we can obtain the time derivative of V_{l1},

$$\begin{aligned}\dot{V}_{l1} = \;& e_{\tilde{R},0}^T\tilde{\omega}_0 + e_{\omega,0}^T\dot{e}_{\omega,0}\\ =\;& e_{\tilde{R},0}^T(-k_1e_{\tilde{R},0}+e_{\omega,0}) - k_2e_{\omega,0}^TM_t^{-1}e_{\omega,0} + e_{\omega,0}^T[\eta_1(\omega_{0,r})\\ & -\eta_1(\omega_0)] + e_{\omega,0}^Td_r\\ \le\;& -k_1\|e_{\tilde{R},0}\|^2 + e_{\tilde{R},0}^Te_{\omega,0} - k_2\lambda(M_t)^{-1}\|e_{\omega,0}\|^2 +\\ & L_1\|e_{\omega,0}\|^2 + e_{\omega,0}^Td_r\\ \le\;& -(k_1-\tfrac{1}{4\rho_1})\|e_{\tilde{R},0}\|^2 - (k_2\lambda(M_t)^{-1}-\rho_1\\ & -\tfrac{1}{4\rho_2}-L_1)\|e_{\omega,0}\|^2 + \rho_2b_r^2\end{aligned} \tag{B.2}$$

Taking $\beta_1 = k_1 - \frac{1}{4\rho_1}$ and $\beta_2 = k_2\lambda(M_t)^{-1} - \rho_1 - \frac{1}{4\rho_2} - L_1$, if the parameters are selected such that $\beta_1 > 0$ and $\beta_2 > 0$, then

$$\dot{V}_{l1} \le -\min(\beta_1,\beta_2)\|(e_{\tilde{R},0}^T, e_{\omega,0}^T)^T\|^2 + \rho_2b_r^2 \tag{B.3}$$

It is seen that $\dot{V}_{l1} < 0$ if $\|(e_{\tilde{R},0}^T, e_{\omega,0}^T)^T\| > \sqrt{\frac{\rho_2}{\min(\beta_1,\beta_2)}}b_r$. The tracking error $e_{\tilde{R},0}$ and $e_{\omega,0}$ satisfy,

$$\begin{aligned}&\|e_{\tilde{R},0}\| \le \|(e_{\tilde{R},0}^T, e_{\omega,0}^T)^T\| \le L_R\\ &\|e_{\omega,0}\| \le \|(e_{\tilde{R},0}^T, e_{\omega,0}^T)^T\| \le L_R\end{aligned} \tag{B.4}$$

Recalling the definition of $e_{\omega,0}$ we arrive at,

$$\|\tilde{\omega}_0\| \le k_1\|e_{\tilde{R},0}\| + \|e_{\omega,0}\| \le (k_1+1)L_R \tag{B.5}$$

Then we consider the boundedness of $\tilde{\tau}_0 = \tau_{0,d} - \bar{\tau}_0$. From the control law we have,

$$\tau_{0,r} - \bar{\tau}_0 = M_t\dot{e}_{\omega,0} + \eta_2(\omega_{0,r}) - \eta_2(\omega_0) \tag{B.6}$$

While from (33) it is concluded that $\tau_{0,d} - \tau_{0,r} = -k_2e_{\omega,0}$, then we have

$$\begin{aligned}\|\tilde{\tau}_0\| = \;& \|-k_1M_t\dot{e}_{\tilde{R},0} + \eta_2(\omega_{0,r}) - \eta_2(\omega_0) - k_2e_{\omega,0}\|\\ \le\;& \|M_t\|k_1\|\tilde{\omega}_0\| + L_3k_1\|e_{\tilde{R},0}\| + k_2\|e_{\omega,0}\|\\ \le\;& (\|M_t\|k_1(k_1+1) + L_3k_1 + k_2)b_r\sqrt{\tfrac{\rho_2}{\min(\beta_1,\beta_2)}}\end{aligned} \tag{B.7}$$

Secondly, we consider the translational part of the (30). For this purpose, we define two variables $\nu_1 = k_5\tilde{p}_{e,0}$ and $\nu_2 = k_5\tilde{p}_{e,0} + \tilde{v}_0$, then define the following Lyapunov candidate,

$$XV_{l2} = \frac{1}{2}\nu_1^T\nu_1 + \nu_2^T\nu_2 \tag{B.8}$$

Combining (37) it can be derived that $\dot{\nu}_2 = k_5(-\nu_1+\nu_2) + \dot{\tilde{v}}_0 \le k_5(-\nu_1+\nu_2) + L_2\|e_{\tilde{R},0}\| + \frac{1}{m_t}\bar{R}_0\tilde{F}_0 + d_t$.

Notice that $\bar{R}_0$ can be expressed as $\bar{R}_0 = \exp(\theta\hat{a})$, where $\theta \in [0,\pi]$ is the eigen-angle of $\bar{R}_0$, and $a \in S^2$ is the eigen-axis of $\bar{R}_0$. Then differentiating V_{l2} yields,

$$\begin{aligned}\dot{V}_{l2} = \;& \nu_1^T\dot{\nu}_1 + \nu_2^T\dot{\nu}_2\\ \le\;& -k_5\|\nu_1\|^2 + k_5\|\nu_2\|^2 + L_2\|e_{\tilde{R},0}\|\|\nu_2\| -\\ & \tfrac{1}{m_t}\cos\theta k_4\|\nu_2\|^2 + \nu_2^Td_t\\ \le\;& -k_5\|\nu_1\|^2 - (\tfrac{1}{m_t}\cos\theta k_4 - k_5 - \tfrac{L_2}{4\rho_3} - \tfrac{1}{4\rho_4})\|\nu_2\|^2\\ & +L_2\rho_3\|e_{\tilde{R},0}\|^2 + \rho_4b_t^2\end{aligned} \tag{B.9}$$

We set $\beta_3 = (\frac{1}{m_t}\cos\theta k_4 - k_5 - \frac{L_2}{4\rho_3} - \frac{1}{4\rho_4})$ and select the parameters appropriately to let $\beta_3 > 0$. Then

$$\dot{V}_{l2} \le -k_5\|\nu_1\|^2 - \beta_3\|\nu_2\|^2 + L_2\rho_3L_R^2 + \rho_4b_t^2 \tag{B.10}$$

It is seen that $\dot{V}_{l2} < 0$ if $\|(\nu_1,\nu_2)\| > \sqrt{\frac{L_2\rho_3L_R^2+\rho_4b_t^2}{\min(k_5,\beta_3)}}$. Therefore we have,

$$\begin{aligned}&\|\tilde{p}_{0,e}\| \le \tfrac{1}{k_5}\|\nu\| \le \tfrac{1}{k_5}\sqrt{\tfrac{L_2\rho_3L_R^2+\rho_4b_t^2}{\min(k_5,\beta_3)}}\\ &\|\tilde{v}_0\| \le \|\nu_1\| + \|\nu_2\| \le 2\sqrt{\tfrac{L_2\rho_3L_R^2+\rho_4b_t^2}{\min(k_5,\beta_3)}}\end{aligned} \tag{B.11}$$

From the control law (34), we can obtain that $\tilde{F}_0$ is bounded by,

$$\|\tilde{F}_0\| \le k_4\|\nu_2\| \le k_4\sqrt{\frac{L_2\rho_3L_R^2+\rho_4b_t^2}{\min(k_5,\beta_3)}}, \tag{B.12}$$

This completes the proof. □

Appendix D. Proof of Proposition 3

Proof. From the definition of V_r it is seen that

$$V_r = \frac{1}{2}tr(I - \bar{R}_{0,e}) + \frac{1}{2}h_{11}\|\bar{\omega}_{0,e}\|^2 \tag{C.1}$$

Combining (47) and (49), the derivative of V_r is derived as,

$$\begin{aligned}\dot{V}_r &= \bar{e}_{R,0}^T\bar{\omega}_0 + h_{11}\bar{\omega}_{0,e}^T\dot{\bar{\omega}}_{0,e}\\ &= \bar{e}_{R,0}^T(\bar{\omega}_{0,d} + \bar{\omega}_{0,e}) - 2k_7h_{11}\bar{\omega}_{0,e}^T\bar{\omega}_{0,e}\\ &= -k_6\|\bar{e}_{R,0}\|^2 + \bar{e}_{R,0}^T\bar{\omega}_{0,e} - 2k_7h_{11}\bar{\omega}_{0,e}^T\bar{\omega}_{0,e}\\ &\le -k_6\|\bar{e}_{R,0}\|^2 + \tfrac{1}{4\rho_5}\|\bar{e}_{R,0}\|^2 + \rho_5\|\bar{\omega}_{0,e}\|^2 - 2k_7h_{11}\|\bar{\omega}_{0,e}\|^2\end{aligned} \tag{C.2}$$

where ρ_5 is a positive constant. Then it is concluded that $\dot{V}_r \le 0$, if k_6 and k_7 satisfy $k_6 > \frac{1}{4\rho_5}$ and $k_7 > \frac{\rho_5}{2h_{11}}$.

Taking the norm of (48) yields,

$$\|\bar{\tau}_0\| \le \|k_7M_t\bar{\omega}_{0,e}\| + \|\hat{\bar{\omega}}_0M_t\bar{\omega}_0\| + \|M_t\dot{\bar{\omega}}_{0,d}\| \tag{C.3}$$

For the second term of the right side of (C.3) the following inequality holds,

$$\|\hat{\bar{\omega}}_0M_t\bar{\omega}_0\| \le L_3\|\bar{\omega}_0\| \tag{C.4}$$

From (47), combing the result of $\|\dot{\bar{e}}_{R,0}\|$ it is seen that,

$$\|M_t\dot{\bar{\omega}}_{0,d}\| \le \|M_t\|k_6\|\dot{\bar{e}}_{R,0}\| \le \|M_t\|k_6\|\bar{\omega}_0\| = L_5\|\bar{\omega}_0\| \tag{C.5}$$

where L_5 is positive constant. Moreover, we can express

$$\|k_7M_t\bar{\omega}_{0,e}\| \le L_6\|\bar{\omega}_{0,e}\| \tag{C.6}$$

where L_6 is a positive constant. Recalling the definition of $\omega_{0,e}$ we have,

$$\|\bar{\omega}_0\|^2 = \|\bar{\omega}_{0,e}\|^2 + 2k_6\bar{\omega}_{0,e}^T\bar{e}_{0,R} + k_6^2\|\bar{e}_{R,0}\|^2 \tag{C.7}$$

Combing (C.3), (C.4) and (C.5), we arrive at,

$$\begin{aligned}&\|\bar{\tau}_0\|^2 \le L_6^2\|\bar{\omega}_{0,e}\|^2 + 2L_6L_7\|\bar{\omega}_{0,e}\|\|\bar{\omega}_0\| + L_7^2\|\bar{\omega}_0\|^2\\ \le\ & L_6^2\|\bar{\omega}_{0,e}\|^2 + \tfrac{L_6L_7}{2\rho_6}\|\bar{\omega}_{0,e}\|^2 + 2L_6L_7\rho_6\|\bar{\omega}_0\|^2 + L_7^2\|\bar{\omega}_0\|^2\end{aligned} \tag{C.8}$$

where $L_7 = L_3 + L_5$. Substituting (C.7) into (C.8) yields,

$$\begin{aligned}&\|\bar{\tau}_0\|^2 \le (L_6^2 + \tfrac{L_6L_7}{2\rho_6} + (L_7^2 + 2L_6L_7\rho_6))\|\bar{\omega}_{0,e}\|^2 +\\ &2k_6(2L_6L_7\rho_6 + L_7^2)\bar{\omega}_{0,e}^T\bar{e}_{0,R} + k_6^2(2L_6L_7\rho_6 + L_7^2)\|\bar{e}_{R,0}\|^2\\ \le\ & [L_6^2 + \tfrac{L_6L_7}{2\rho_6} + (L_7^2 + 2L_6L_7\rho_6) +\\ &\tfrac{2k_6(2L_6L_7\rho_6 + L_7^2)}{4\rho_7}]\|\bar{\omega}_{0,e}\|^2 +\\ &\left[k_6^2(2L_6L_7\rho_6 + L_7^2) + 2\rho_7k_6(2L_6L_7\rho_6 + L_7^2)\right]\|\bar{e}_{R,0}\|^2\\ :=\ & L_8\|\bar{\omega}_{0,e}\|^2 + L_9\|\bar{e}_{R,0}\|^2\end{aligned} \tag{C.9}$$

where ρ_6 and ρ_7 are positive constants.

Secondly, from (C.2), (C.9) and the definition of N_r, it is concluded that,

$$\begin{aligned}\dot{V}_r + N_r \le\ & -(k_6 - \tfrac{1}{4\rho_5} - q_{11} - r_1L_8)\|\bar{e}_{R,0}\|^2 -\\ & (2k_7h_{11} - \rho_5 - q_{12} - r_1L_9)\|\bar{\omega}_{0,e}\|^2\end{aligned} \tag{C.10}$$

Then if the parameters are appropriately selected, we arrive at $\dot{V}_r + N_r \le 0$.

Thirdly, as $\|\bar{e}_{R,0}\|^2 \le \mathrm{tr}(I - \bar{R}_{0,e})$, we have

$$\|\bar{e}_{R,0}\|^2 \le 2\epsilon_r, \forall\bar{\zeta}_r \in \Omega_r \tag{C.11}$$

Then from (C.9) it is seen that

$$\|\bar{\tau}_0\| \le \sqrt{\max\left(\frac{L_9}{2}, \frac{2L_8}{h_{11}}\right)\epsilon_r} = \bar{\tau}_m, \forall\bar{\zeta}_r \in \Omega_r \tag{C.12}$$

This means that $\bar{\tau}_0 \in \bar{S}_7$ for all $\bar{\zeta}_r \in \Omega_r$. This completes the proof. □

Appendix E. Proof of Proposition 4

Proof. Substituting the control law (52) into the nominal dynamics of the load (21), and considering the definition of $v_{0,e}$, we have,

$$\dot{\bar{p}}_{0,e} = \bar{v}_{0,d} + \bar{v}_{0,e}, \dot{\bar{v}}_{0,e} = -k_9 \bar{v}_{0,e} \tag{D.1}$$

From the definition of V_t it is seen that

$$V_t = \frac{1}{2} h_{21} \|\bar{p}_{0,e}\|^2 + \frac{1}{2} h_{22} \|\bar{v}_{0,e}\|^2 \tag{D.2}$$

Then the time derivative of V_t can be derived as,

$$\begin{aligned} \dot{V}_t = \;& h_{21} \bar{p}_{0,e}^T \dot{\bar{p}}_{0,e} + h_{22} \bar{v}_{0,e}^T \dot{\bar{v}}_{0,e} \\ = \;& h_{21} \bar{p}_{0,e}^T (\bar{v}_{0,e} + \bar{v}_{0,d}) + h_{22} \bar{v}_{0,e}^T (-k_9 \bar{v}_{0,e}) \\ \leq \;& -k_8 h_{21} \|\bar{p}_{0,e}\|^2 - k_9 h_{22} \|\bar{v}_{0,e}\|^2 \\ & + h_{21} \tfrac{1}{4\rho_8} \|\bar{p}_{0,e}\|^2 + h_{21} \rho_8 \|\bar{v}_{0,e}\|^2 \end{aligned} \tag{D.3}$$

where ρ_8 is a positive constant. It is seen that if k_8 and k_9 satisfy $k_8 > \frac{1}{4\rho_8}$ and $k_9 > \frac{h_{21}}{h_{22}} \rho_8$, then $\dot{V}_t \leq 0$, which shows the set Ω_t is an invariant set.

Next, from the definition of N_t we have,

$$\begin{aligned} \dot{V}_t + N_t \quad \leq\; & -k_8 h_{21} \|\bar{p}_{0,e}\|^2 - k_9 h_{22} \|\bar{v}_{0,e}\|^2 + \\ & h_{21} \tfrac{1}{4\rho_8} \|\bar{p}_{0,e}\|^2 + h_{21} \rho_8 \|\bar{v}_{0,e}\|^2 + q_{21} \|\bar{p}_{0,e}\|^2 + \\ & q_{22} \|\bar{v}_0\|^2 + r_2 m_t^2 [(k_8 + k_9)^2 \|\bar{v}_{0,e}\|^2 - \\ & 2k_8^2 (k_8 + k_9) \bar{p}_{0,e}^T \bar{v}_{0,e} + k_8^4 \|\bar{p}_{0,e}\|^2] \\ = \;& -\Big(k_8 h_{21} - (h_{21} - 2k_8^2 r_2 m_t^2 (k_8 + k_9)) \tfrac{1}{4\rho_8} - \\ & q_{21} - r_2 m_t^2 k_8^4 \Big) \|\bar{p}_{0,e}\|^2 - (k_9 h_{22} - (h_{21} - \\ & 2k_8^2 r_2 m_t^2 (k_8 + k_9)) \rho_8 - q_{22} - r_2 m_t^2 (k_8 + k_9)^2 \Big) \|\bar{v}_{0,e}\|^2 \end{aligned} \tag{D.4}$$

If the parameters satisfy $k_8 h_{21} - (h_{21} - 2k_8^2 r_2 m_t^2 (k_8 + k_9)) \frac{1}{4\rho_8} - q_{21} - r_2 m_t^2 k_8^4 > 0$ and $(k_9 h_{22} - (h_{21} - 2k_8^2 r_2 m_t^2 (k_8 + k_9)) \rho_8 - q_{22} - r_2 m_t^2 (k_8 + k_9)^2) > 0$, then it is concluded that $\dot{V}_t + N_t \leq 0$.

It is seen that if $\bar{\zeta}_t \in \Omega_t$, the following inequality holds,

$$\begin{aligned} & \|k_9 \bar{v}_{0,e} + k_8 \bar{v}_{0,e} - k_8^2 \bar{p}_{0,e}\| \\ \leq \;& k_9 \|\bar{v}_{0,e}\| + k_8 \|\bar{v}_{0,e}\| + k_8^2 \|\bar{p}_{0,e}\| \\ \leq \;& (k_8 + k_9) \sqrt{\tfrac{2\epsilon_t^2}{h_{21}}} + k_8^2 \sqrt{\tfrac{2\epsilon_t^2}{h_{22}}} \end{aligned} \tag{D.5}$$

Furthermore, we have,

$$\|\bar{R}_0^T (k_9 \bar{v}_{0,e} + k_8 \bar{v}_{0,e} - k_8^2 \bar{p}_{0,e})\| = \|k_9 \bar{v}_{0,e} + k_8 \bar{v}_{0,e} - k_8^2 \bar{p}_{0,e}\| \tag{D.6}$$

Combining (D.5) and (D.6), and from the definition of ϵ_t, we have,

$$\begin{aligned} & m_t \|\bar{R}_0^T (k_9 \bar{v}_{0,e} + k_8 \bar{v}_{0,e} - k_8^2 \bar{p}_{0,e})\| \leq F_{m,z} - \Delta_F, \\ & m_t g \sqrt{1 - L_l^2} + m_t \|\bar{R}_0^T (k_9 \bar{v}_{0,e} + k_8 \bar{v}_{0,e} - k_8^2 \bar{p}_{0,e})\| \leq \bar{F}_{m,h} \end{aligned} \tag{D.7}$$

Recalling (52) and (44), we can conclude that $\bar{F}_0 \in \bar{S}_5$. □

Appendix F. Proof of Theorem 1

Proof. First, let us prove the feasibility of the MPC problem recursively. Assume at a sampling instant t_k the solution for the optimal control problem exists, denoted by $\bar{u}_0^*(s), s \in [t_k, t_k + \Gamma]$. According to the state constraints definition, at the time instant t_k, the state $\bar{\zeta}$ stays in the terminal region under the control of $\bar{u}_0^*(t_k)$.

Then for the time interval $[t_{k+1}, t_{k+1} + \Gamma]$ we can construct the following solution for the optimal control problem (42),

$$\bar{u}_{0,f} = \begin{cases} \bar{u}_0^*(s), s \in [t_{k+1}, t_k + \Gamma] \\ \bar{u}_{0,ter}(s), s \in (t_k + \Gamma, t_{k+1} + \Gamma] \end{cases} \tag{E.1}$$

where $\bar{u}_{0,ter} = (\bar{F}_{0,ter}, \bar{\tau}_{0,ter})$ is determined by (48) and (52). According to Proposition 3 and Proposition 4, $\bar{u}_{0,ter}$ defined by (48) and (52) is a terminal controller, which means that $\bar{u}_{0,ter}(s) \in \bar{U}$ for all $s \in (t_k + \Gamma, t_{k+1} + \Gamma]$. Because the control is a terminal control, it is seen that the state will be kept in terminal region at time $t_{k+1} + \Gamma$, which means that under the control $\bar{u}_{0,ter}$, we have,

$$\bar{\zeta}(t_{k+1} + \Gamma) \in \Omega_r \times \Omega_t \tag{E.2}$$

Therefore, we can conclude that $\bar{u}_{0,f}(s), s \in [t_{k+1}, t_{k+1}+\Gamma]$ is a feasible solution of (42). The feasibility of (42) can thus be guaranteed recursively in this way.

Next we consider the convergence of the MPC problem.

We define the following Lyapunov candidate of the closed loop nominal system,

$$\bar{V} = J(\bar{\zeta}, \bar{u}_0) \tag{E.3}$$

Then the difference of $\bar{V}$ from the time instant t_k to the time instant t_{k+1} is given by,

$$\begin{aligned}
&\Delta V = \bar{V}(t_{k+1}) - \bar{V}(t_k)\\
&= \int_{t_{k+1}}^{t_{k+1}+\Gamma} \left[N_r\left(\bar{\zeta}_r(s), \bar{\tau}_0(s)\right) + N_t\left(\bar{\zeta}_t(s), \bar{F}_0(s)\right)\right] ds\\
&- \int_{t_k}^{t_k+\Gamma} \left[N_r\left(\bar{\zeta}_r(s), \bar{\tau}_0(s)\right) + N_t\left(\bar{\zeta}_t(s), \bar{F}_0(s)\right)\right] ds\\
&+ V_r\left(\bar{\zeta}_r(t_{k+1}+\Gamma)\right) + V_t\left(\bar{\zeta}_t(t_{k+1}+\Gamma)\right) -\\
&V_r\left(\bar{\zeta}_r(t_k+\Gamma)\right) - V_t\left(\bar{\zeta}_t(t_k+\Gamma)\right)\\
&= \int_{t_k+\Gamma}^{t_{k+1}+\Gamma} \left[N_r\left(\bar{\zeta}_r(s), \bar{\tau}_0(s)\right) + N_t\left(\bar{\zeta}_t(s), \bar{F}_0(s)\right)\right] ds\\
&- \int_{t_k}^{t_{k+1}} \left[N_r\left(\bar{\zeta}_r(s), \bar{\tau}_0(s)\right) + N_t\left(\bar{\zeta}_t(s), \bar{F}_0(s)\right)\right] ds\\
&+ V_r\left(\bar{\zeta}_r(t_{k+1}+\Gamma)\right) + V_t\left(\bar{\zeta}_t(t_{k+1}+\Gamma)\right) -\\
&V_r\left(\bar{\zeta}_r(t_k+\Gamma)\right) - V_t\left(\bar{\zeta}_r(t_k+\Gamma)\right)
\end{aligned} \tag{E.4}$$

From Proposition 3 and 4, integrating $\dot{V}_r + \dot{V}_t + N_t + N_r$ over $[t_k+\Gamma, t_{k+1}+\Gamma]$ yields,

$$\begin{aligned}
&\int_{t_k+\Gamma}^{t_{k+1}+\Gamma} \left[N_r\left(\bar{\zeta}_r(s)\right) + N_t\left(\bar{\zeta}_t(s)\right)\right] ds\\
&+ V_r\left(\bar{\zeta}_r(t_{k+1}+\Gamma)\right) + V_t\left(\bar{\zeta}_t(t_{k+1}+\Gamma)\right) -\\
&V_r\left(\bar{\zeta}_r(t_k+\Gamma)\right) - V_t\left(\bar{\zeta}_t(t_k+\Gamma)\right) \le 0
\end{aligned} \tag{E.5}$$

Substituting (E.5) into (E.4) yields,

$$\Delta V \le 0 \tag{E.6}$$

Therefore, it is concluded that the closed loop nominal system is asymptotically stable at origin. Then there exists a class $\mathcal{KL}$ function $\alpha_1(\cdot)$ such that,

$$\bar{\zeta}(t) \le \alpha_1(\bar{\zeta}(0), t), \forall t > 0 \tag{E.7}$$

From Lemma 3 it is seen that there exists a class $\mathcal{K}$ function $\alpha_2(\cdot)$ such that,

$$\|(b_r, b_t)\| \le \alpha_2(\|(b_{0r}, b_{0t}, b_a)\|), \forall t > 0 \tag{E.8}$$

Moreover, from Proposition 2, it is seen that there exist class $\mathcal{K}$ functions $\alpha_3(\cdot)$ and $\alpha_4(\cdot)$ such that,

$$\|\tilde{\zeta}_r\| \le \alpha_3(b_r), \|\tilde{\zeta}_t\| \le \alpha_4(\|(b_r, b_t)\|), \forall t > 0 \tag{E.9}$$

Thus there exists a class $\mathcal{K}$ function $\alpha_5(\cdot)$ such that,

$$\|\tilde{\zeta}\| \le \alpha_5(\|(b_{0r}, b_{0t}, b_a)\|), \forall t > 0 \tag{E.10}$$

Then combining the result of (E.7) and (E.10), it is seen that $\forall t > 0$,

$$\|\zeta\| \le \|\bar{\zeta}(t)\| + \|\tilde{\zeta}(t)\| \le \alpha_5(\|(b_{0r}, b_{0t}, b_a)\|) + \alpha_1(\bar{\zeta}(0), t) \tag{E.11}$$

which shows that the entire system is ISS with respect to the disturbances. □

Supplementary material

Supplementary material associated with this article can be found, in the online version, at 10.1016/j.apm.2022.05.013

References

[1] Y. Yu, X. Ding, A global tracking controller for underactuated aerial vehicles: design, analysis, and experimental tests on quadrotor, IEEE/ASME Trans. Mechatron. 21 (5) (2016) 2499–2511.

[2] Y. Yu, X. Ding, Trajectory linearization control on so(3) with application to aerial manipulation, J. Franklin Inst. 355 (15) (2018) 7072–7097.

[3] X. Liang, Y. Fang, N. Sun, H. Lin, A novel energy-coupling-based hierarchical control approach for unmanned quadrotor transportation systems, IEEE/ASME Trans. Mechatron. 24 (1) (2019) 248–259, doi:10.1109/TMECH.2019.2891083.

[4] J. Thomas, G. Loianno, K. Sreenath, V. Kumar, Toward image based visual servoing for aerial grasping and perching, in: 2014 IEEE International Conference on Robotics and Automation (ICRA), 2014, pp. 2113–2118.

[5] S. Hamaza, I. Georgilas, G. Heredia, A. Ollero, T. Richardson, Design, modeling, and control of an aerial manipulator for placement and retrieval of sensors in the environment, J. Field Rob. 37 (7) (2020) 1224–1245.

[6] Y. Yu, V. Lippiello, 6D pose task trajectory tracking for a class of 3d aerial manipulator from differential flatness, IEEE Access 7 (2019) 52257–52265, doi:10.1109/ACCESS.2019.2910379.

[7] M. Ryll, G. Muscio, F. Pierri, E. Cataldi, G. Antonelli, F. Caccavale, D. Bicego, A. Franchi, 6D interaction control with aerial robots: the flying end-effector paradigm, Int. J. Rob. Res. 38 (9) (2019) 1045–1062.

[8] T. Lee, Geometric control of quadrotor uavs transporting a cable-suspended rigid body, IEEE Trans. Control Syst. Technol. 26 (1) (2018) 255–264, doi:10.1109/TCST.2017.2656060.
[9] H. Nguyen, S. Park, J. Park, D. Lee, A novel robotic platform for aerial manipulation using quadrotors as rotating thrust generators, IEEE Trans. Rob. 34 (2) (2018) 353–369, doi:10.1109/TRO.2018.2791604.
[10] B. Shirani, M. Najafi, I. Izadi, Cooperative load transportation using multiple UAVs, Aerosp. Sci. Technol. 84 (2019) 158–169.
[11] R. Chai, A. Tsourdos, A. Savvaris, Y. Xia, S. Chai, Real-time reentry trajectory planning of hypersonic vehicles: a two-step strategy incorporating fuzzy multiobjective transcription and deep neural network, IEEE Trans. Ind. Electron. 67 (8) (2020) 6904–6915, doi:10.1109/TIE.2019.2939934.
[12] R. Chai, A. Tsourdos, A. Savvaris, S. Chai, Y. Xia, C.L.P. Chen, Six-dof spacecraft optimal trajectory planning and real-time attitude control: a deep neural network-based approach, IEEE Trans Neural Netw Learn Syst 31 (11) (2020) 5005–5013, doi:10.1109/TNNLS.2019.2955400.
[13] Z. Zheng, X. Su, T. Jiang, J.-S. Huang, Robust dynamic geofencing attitude control for quadrotor systems, IEEE Trans. Ind. Electron. (2022), doi:10.1109/TIE.2022.3159919. 1–1.
[14] R. Chai, A. Savvaris, A. Tsourdos, S. Chai, Y. Xia, Unified multiobjective optimization scheme for aeroassisted vehicle trajectory planning, Journal of Guidance, Control, and Dynamics 41 (7) (2018) 1521–1530, doi:10.2514/1.G003189.
[15] Y. Yu, J. Guo, C.K. Ahn, Z. Xiang, Neural adaptive distributed formation control of nonlinear multi-uavs with unmodeled dynamics, IEEE Trans. Neural Netw. Learn. Syst. (2022) 1–7, doi:10.1109/TNNLS.2022.3157079.
[16] W. Langson, I. Chryssochoos, S. Rakovic, D. Mayne, Robust model predictive control using tubes, Automatica 40 (1) (2004) 125–133.
[17] F.D. Brunner, M. Heemels, F. Allgwer, Robust self-triggered MPC for constrained linear systems: a tube-based approach, Automatica 72 (2016) 73–83.
[18] X. Zhang, W. Pan, R. Scattolini, S. Yu, X. Xu, Robust tube-based model predictive control with Koopman operators, Automatica 137 (2022) 110114.
[19] M. Yue, X. Hou, X. Zhao, X. Wu, Robust tube-based model predictive control for lane change maneuver of tractor-trailer vehicles based on a polynomial trajectory, IEEE Transactions on Systems, Man, and Cybernetics: Systems (2018) 1–9.
[20] Y. Gao, A. Gray, H.E. Tseng, F. Borrelli, A tube-based robust nonlinear predictive control approach to semiautonomous ground vehicles, Veh. Syst. Dyn. 52 (6) (2014) 802–823.
[21] Z. Sun, L. Dai, K. Liu, Y. Xia, K.H. Johansson, Robust MPC for tracking constrained unicycle robots with additive disturbances, Automatica 90 (2018) 172–184.
[22] A. Nikou, D.V. Dimarogonas, Decentralized tube-based model predictive control of uncertain nonlinear multiagent systems, Int. J. Robust Nonlinear Control 29 (10) (2019) 2799–2818, doi:10.1002/rnc.4522.
[23] A. Nikou, C.K. Verginis, D.V. Dimarogonas, A tube-based mpc scheme for interaction control of underwater vehicle manipulator systems, in: 2018 IEEE/OES Autonomous Underwater Vehicle Workshop (AUV), 2018, pp. 1–6, doi:10.1109/AUV.2018.8729801.
[24] D. Six, S. Briot, A. Chriette, P. Martinet, The kinematics, dynamics and control of a flying parallel robot with three quadrotors, IEEE Rob. Autom. Lett. 3 (1) (2018) 559–566, doi:10.1109/LRA.2017.2774920.
[25] G. Cardona, D. Tellez-Castro, E. Mojica-Nava, Cooperative transportation of a cable-suspended load by multiple quadrotors, IFAC-PapersOnLine 52 (20) (2019) 145–150. 8th IFAC Workshop on Distributed Estimation and Control in Networked Systems NECSYS 2019
[26] P.O. Pereira, D.V. Dimarogonas, Control framework for slung load transportation with two aerial vehicles, in: 2017 IEEE 56th Annual Conference on Decision and Control (CDC), 2017, pp. 4254–4259, doi:10.1109/CDC.2017.8264286.
[27] A. Tagliabue, M. Kamel, R. Siegwart, J. Nieto, Robust collaborative object transportation using multiple mavs, Int. J. Rob. Res. 38 (9) (2019) 1020–1044.
[28] M.A. Santos, A. Ferramosca, G.V. Raffo, Tube-based mpc with nonlinear control for load transportation using a uav, IFAC-PapersOnLine 51 (25) (2018) 459–465. 9th IFAC Symposium on Robust Control Design ROCOND 2018
[29] S. Yu, C. Maier, H. Chen, F. Allgwer, Tube mpc scheme based on robust control invariant set with application to lipschitz nonlinear systems, Systems & Control Letters 62 (2) (2013) 194–200.
[30] A. Majumdar, R. Tedrake, Funnel libraries for real-time robust feedback motion planning, Int. J. Rob. Res. 36 (8) (2017) 947–982.
[31] S. Kousik, S. Vaskov, M. Johnson-Roberson, R. Vasudevan, Safe trajectory synthesis for autonomous driving in unforeseen environments, in: Dynamic Systems and Control Conference, volume 1, 2017.
[32] S. Kim, D. Falanga, D. Scaramuzza, Computing the forward reachable set for a multirotor under first-order aerodynamic effects, IEEE Rob. Autom. Lett. 3 (4) (2018) 2934–2941.
[33] F. Oliva-Palomo, A. Sanchez-Orta, P. Castillo, H. Alazki, Nonlinear ellipsoid based attitude control for aggressive trajectories in a quadrotor: closed-loop multi-flips implementation, Control Eng Pract 77 (2018) 150–161.
[34] C.G. Mayhew, R.G. Sanfelice, A.R. Teel, Quaternion-based hybrid control for robust global attitude tracking, IEEE Trans Automat Contr 56 (11) (2011) 2555–2566.
[35] D.E. Chang, On controller design for systems on manifolds in euclidean space, Int. J. Robust Nonlinear Control 28 (16) (2018) 4981–4998, doi:10.1002/rnc.4294.
[36] T. Lee, Geometric tracking control of the attitude dynamics of a rigid body on SO(3), in: Proc. American Control Conference, 2011, pp. 1200–1205. San Francisco, CA
[37] M.M. Polycarpou, Stable adaptive neural control scheme for nonlinear systems, IEEE Trans. Automat. Contr. 41 (3) (1996) 447–451, doi:10.1109/9.486648.
[38] T. Chen, J. Shan, A novel cable-suspended quadrotor transportation system: from theory to experiment, Aerosp. Sci. Technol. 104 (2020) 105974, doi:10.1016/j.ast.2020.105974.
[39] P. Pounds, R. Mahony, P. Corke, Modelling and control of a large quadrotor robot, Control Eng. Practice 18 (7) (2010) 691–699.
[40] C. Chron, A. Dennis, V. Semerjyan, Y. Chen, A multifunctional HIL testbed for multirotor VTOL UAV actuator, in: Proceedings of 2010 IEEE/ASME International Conference on Mechatronic and Embedded Systems and Applications, 2010, pp. 44–48, doi:10.1109/MESA.2010.5552032.
[41] ACADO Toolkit Homepage, 20092013. http://www.acadotoolkit.org.
[42] K.K. Dhiman, M. Kothari, A. Abhishek, Autonomous load control and transportation using multiple quadrotors, Journal of Aerospace Information Systems 17 (8) (2020) 417–435, doi:10.2514/1.I010787.
[43] Stanford Artificial Intelligence Laboratory, Robotic operating system, https://www.ros.org.